

UCRHEP-T200

August 1997

Implications of a $W^+W^-(ZZ) - \text{Higgs} - t\bar{c}$ Interaction for $e^+e^- \rightarrow t\bar{c}\nu_e\bar{\nu}_e$, $t\bar{c}e^+e^-$, $t\bar{c}Z$ and for $t \rightarrow cW^+W^-$, cZZ in a Two Higgs Doublet Model

S. Bar-Shalom^a, G. Eilam^b, A. Soni^c and J. Wudka^a

^a Physics Dept., University of California, Riverside CA 92521, USA.

^b Physics Dept., Technion-Israel Inst. of Tech., Haifa 32000, Israel.

^c Physics Dept., Brookhaven Nat. Lab., Upton NY 11973, USA.

Abstract

Abstract: The Standard Model with one extra Higgs doublet may give rise to enhanced *tree-level* flavor-changing-scalar coupling of a neutral Higgs to a pair of top-charm quarks. This coupling may drive a large *tree-level* effective $W^+W^-(ZZ) - \text{Higgs} - t\bar{c}$ interaction. As a result we find that the reactions $e^+e^- \rightarrow t\bar{c}\nu_e\bar{\nu}_e$, $t\bar{c}e^+e^-$, $t\bar{c}Z$ and the two rare top decays $t \rightarrow cW^+W^-$, $t \rightarrow cZZ$ become very sensitive probes of such an effective interaction. The most promising ones, $e^+e^- \rightarrow t\bar{c}\nu_e\bar{\nu}_e$, $t\bar{c}e^+e^-$, may yield several hundreds and up to thousands of such events at the Next Linear Collider with a center of mass energy of $\sqrt{s} = 0.5\text{--}2$ TeV if the mass of the lightest neutral Higgs is a few hundred GeV. The rare decays $t \rightarrow cW^+W^-$ and $t \rightarrow cZZ$ may be accessible at the LHC if the mass of the lightest neutral Higgs lies in the narrow window $150 \text{ GeV} \lesssim m_h \lesssim 200 \text{ GeV}$.

1 Introduction

Understanding the nature of the scalar sector, which still remains one of the great mysteries in electroweak theories, and searching for flavor-changing (FC) currents are clearly important goals of the next generation of high energy colliders [1].

Although the Standard Model (SM) with only one scalar doublet is in good agreement with existing data, it is still useful to examine consequences of simple extensions of the SM. Indeed, the simplest possible extension of the scalar potential, which contains two Higgs doublets, exhibits rich new phenomena. In particular it may give rise to new tree-level FC couplings of a spin 0 particle with fermions [2].

In the SM there are no tree-level flavor-changing-neutral-currents (FCNC). At the one loop level, FC transitions involving external up quarks are much more suppressed than those involving external down quarks. The effects for the up quarks are driven by virtual exchanges of down quarks for which the GIM mechanism is much more effective since the mass splitting between the down quarks is a lot less than amongst the charge 2/3 quarks. Therefore, the search for large signatures of FCNC involving the up quarks is extremely important as it may serve as a unique test of the SM. As is well known, though there are stringent experimental constraints against the existence of tree level flavor-changing-scalar (FCS) transitions involving the light quarks [3, 4, 5], analogous constraints involving the top quark are essentially non-existent.

As mentioned above, a mild extension of the SM in which one extra scalar doublet is added, allows for large, tree-level FCS interactions [2]. These are often forbidden by the imposition of an *ad-hoc* symmetry [3]; if this symmetry is not imposed, however, one arrives at a version of the two-Higgs doublet model (2HDM) wherein the up and down-type quarks are allowed simultaneously to couple to more than one scalar doublet [2] leading to tree-level FC vertices. In the context of such new interactions, the severe experimental constraints involving FC couplings of the light quarks can be satisfied by requiring that FCS interactions are proportional to the square root of masses of the fermions participating at the vertex [4]. A specific realization of these ideas, the Cheng-Sher Ansatz (CSA), assumes that the FC coupling of a scalar to top and up (charm) quark is proportional to $\sqrt{m_t m_u}/m_W$ (or $\sqrt{m_t m_c}/m_W$). In this scenario the large top mass makes it much more susceptible to FC transitions. This possibility has led various authors to stress the importance of searching for tree-level FCS interactions involving the top-quark, especially the top-charm ones [2,5–9]. Our study indicates that experimental investigations of the reactions $e^+ + e^- \rightarrow t\bar{c}\nu_e\bar{\nu}_e$; $\bar{t}c\nu_e\bar{\nu}_e$; $t\bar{c}e^+e^-$; $\bar{t}ce^+e^-$; $Zt\bar{c}$; $Z\bar{t}c$ and of the rare top decays $t \rightarrow W^+W^-c$; ZZc will be very useful in this regard.

The paper is organized as follows: in section 2 we briefly describe the key features of a 2HDM with tree-level FC couplings, often called Model III. The possibility of producing $t\bar{c}$ pairs via WW and ZZ fusion in the next linear collider (NLC) is investigated in section 3. In section 4 we discuss the reaction $e^+e^- \rightarrow Zt\bar{c}$. In section 5 we examine the two rare top decays $t \rightarrow W^+W^-c$ and $t \rightarrow ZZc$ and in section 6 we summarize our results and make some parting comments.

2 2HDM With Tree-Level FC Couplings (Model III)

In a most general version of the 2HDM (which allows tree-level FCS couplings) one can always choose a basis of scalar fields where only one doublet acquires a vacuum expectation value (VEV) (for a brief review see [5]):

$$\langle \phi_1^0 \rangle = \frac{v}{\sqrt{2}} , \quad \langle \phi_2^0 \rangle = 0 . \quad (1)$$

We refer to this type of a 2HDM as Model III.

With this choice ϕ_1 corresponds to the usual SM scalar doublet and all the new FC couplings are associated with the ϕ_2 doublet. The spectrum of the scalar sector then consists of a charged scalar and its conjugate H^\pm , and three neutral Higgs particles which we will denote by h, H (the scalar mass eigenstates) and A (the pseudoscalar mass eigenstate). In terms of the original doublets one has:

$$\begin{aligned} H &= \sqrt{2} \left[\left(\text{Re} \phi_1^0 - v \right) \cos \tilde{\alpha} + \text{Re} \phi_2^0 \sin \tilde{\alpha} \right] , \\ h &= \sqrt{2} \left[- \left(\text{Re} \phi_1^0 - v \right) \sin \tilde{\alpha} + \text{Re} \phi_2^0 \cos \tilde{\alpha} \right] , \\ A &= \sqrt{2} \left(-\text{Im} \phi_2^0 \right) . \end{aligned} \quad (2)$$

The masses of the neutral and charged Higgs bosons as well as the mixing angle $\tilde{\alpha}$ are free parameters of the model.¹ The pseudoscalar A which does not couple to gauge bosons and the charged Higgs particles of the model do not play any role in our reactions and therefore their masses are not relevant for the present analysis.

Although with the above basis for Model III, in which $\langle \phi_2^0 \rangle = 0$ at the tree-level, introducing large splitting between the masses of the two Higgs particles h and H (in some cases we will take $m_H - m_h > 500$ GeV) can become slightly unnatural for large values of $\tilde{\alpha}$, this is not the case in a more general flavor-changing 2HDM where both doublets can acquire a non-vanishing VEV. In that more general case, $\tan \beta \equiv v_2/v_1$ appears as an additional free parameter of the model. Adopting $\tan \beta \neq 0$ will not affect our predictions in this paper, while, due to the presence of this additional free parameter $\tan \beta$, large values of $\tilde{\alpha}$ can be accommodated without much difficulty in this framework regardless of the degree of splitting between the two Higgs masses. Note also that $\tan \beta$ will not enter the FC couplings of a neutral Higgs to fermions as those are governed by the couplings λ_{ij} to be defined below. We therefore wish to emphasize that we are not trying to advocate the existence of the above particularly simple realization of a FC 2HDM where one of the Higgs doublets does not acquire a VEV, instead, for its simplicity, we are using it as an illustrative scenario to estimate the size of a possible FC effect in our reactions. Thus, in what follows, we will always choose the mass of the lighter Higgs, h , to be in the range $50 \text{ GeV} \lesssim m_h \lesssim 1 \text{ TeV}$ while, in most instances, we will set the heavy Higgs (H)

¹We use $\tilde{\alpha}$ instead of α to avoid confusion with the fine-structure constant.

mass to be $m_H = 1$ TeV independent of the choice of mixing angle $\tilde{\alpha}$.²

The FC part of the Yukawa Lagrangian in Model III is given by [2, 5]:

$$\mathcal{L}_Y^{FC} = \xi_{ij}^U \bar{Q}_{i,L} \tilde{\phi}_2 U_{j,R} + \xi_{ij}^D \bar{Q}_{i,L} \phi_2 D_{j,R} + h.c. , \quad (3)$$

where ϕ_2 denotes the second scalar doublet, $\tilde{\phi}_2 \equiv i\tau_2 \phi_2$, Q stands for the quark doublets, and U and D for charge 2/3 and (-1/3) quarks singlets; $i, j = 1, 2, 3$ are the generation indices and ξ are 3×3 matrices parameterizing the strength of FC neutral scalar vertices. Following Cheng and Sher [4] we choose the parameterization:

$$\xi_{ij}^{U,D} = g_W \frac{\sqrt{m_i m_j}}{m_W} \lambda_{ij} . \quad (4)$$

In this scenario all our ignorance regarding the FCS vertices is contained in the couplings λ_{ij} which are free parameters to be deduced from experiments. The experimental constraints on the λ_{ij} are rather mild: for example, if $\lambda_{sd}, \lambda_{bd}$ and λ_{uc} are kept below ~ 0.1 , then Model III is compatible with the existing low energy experimental measurements as long as the other FC couplings (i.e., those involving the top quark) are not much larger than 1 [5]. In particular, if the first generation FC couplings are not related to the FC couplings of the second and third generations (there is no good reason to believe that such a relation exists) then $\lambda_{tc} = \lambda_{ct} \sim O(1)$, or even somewhat bigger, is not ruled out³ by existing experiments [5]. This has major consequences on our analysis in this paper as all the reactions investigated here scale like λ_{tc}^2 .

For simplicity, we choose $\lambda_{tc} = \lambda_{ct} = \lambda$ and we furthermore break λ into its real and imaginary parts, $\lambda = \lambda_R + i\lambda_I$. Then, within the CSA, the relevant terms of the Model III Lagrangian become:

$$\mathcal{L}_{\mathcal{H}tc} = -\frac{g_W}{\sqrt{2}} \frac{\sqrt{m_t m_c}}{m_W} f_{\mathcal{H}} \mathcal{H} \bar{t} (\lambda_R + i\lambda_I \gamma_5) c , \quad (5)$$

$$\mathcal{L}_{\mathcal{H}VV} = -g_W m_W C_V c_{\mathcal{H}} \mathcal{H} g_{\mu\nu} V^\mu V^\nu , \quad (6)$$

where here and throughout the paper $\mathcal{H} = h$ or H and $V = W$ or Z and⁴:

$$f_{h;H} \equiv \cos \tilde{\alpha}; \sin \tilde{\alpha} , \quad (7)$$

$$c_{h;H} \equiv \sin \tilde{\alpha}; -\cos \tilde{\alpha} , \quad (8)$$

$$C_{W;Z} \equiv 1; m_Z^2/m_W^2 . \quad (9)$$

²Note that the onset of a strongly interacting Higgs sector corresponds to the breakdown of tree-level unitarity and also to the condition that the radiative corrections to the Higgs mass are of order 100%, i.e., $\delta m_H \approx m_H$. Much like in the SM case, this will occur when $m_H \sim 4\pi v \sim 3$ TeV. Therefore, although taking $m_H = 1$ TeV is somewhat close to the above limit, still, it is unlikely to enter the strongly interacting Higgs domain.

³ λ_{tu} is also not well constrained from existing experiments. The Cheng and Sher Ansatz (4) does, of course, imply much smaller tu coupling compared to the tc one due to the up-charm mass difference.

⁴ $V = W^+, W^-$ or Z ; in most instances the appropriate choice can be fixed by inspection. If necessary we will denote $V^1 = W^+, V^2 = W^-$ or $V^1 = V^2 = Z$.

The amplitude for the reaction $VV - \mathcal{H} - t\bar{c}$, $\bar{t}c$ is proportional to $\sin 2\tilde{\alpha}$ for *both* $\mathcal{H} = h$ and H , and will vanish for $\tilde{\alpha} = 0, \pi/2$. When $\tilde{\alpha} = \pi/4$ (i.e., equal mixing between $\text{Re}\phi_1^0 - \text{Re}\phi_2^0$) the h and H contributions interfere destructively and cancel out in the limit $m_H \rightarrow m_h$. The presence of this “GIM-like” cancellation reflects the fact that all complete calculations should include both neutral scalars. The maximum of the cross section is not reached at $\tilde{\alpha} = \pi/4$ since the scalar widths also depend on this parameter.

We will also need the $\mathcal{H}t\bar{t}$ couplings within Model III:

$$\mathcal{L}_{\mathcal{H}t\bar{t}} = -\frac{g_W}{\sqrt{2}} \frac{m_t}{m_W} \mathcal{H}\bar{t}(a_{\mathcal{H}} + ib_{\mathcal{H}}\gamma_5)t, \quad (10)$$

where

$$a_h = -\frac{1}{\sqrt{2}} \sin \tilde{\alpha} + \cos \tilde{\alpha} \lambda_R, \quad b_h = \cos \tilde{\alpha} \lambda_I, \quad (11)$$

$$a_H = \frac{1}{\sqrt{2}} \cos \tilde{\alpha} + \sin \tilde{\alpha} \lambda_R, \quad b_H = \sin \tilde{\alpha} \lambda_I, \quad (12)$$

and for simplicity we set $\lambda_{tt} = \lambda_{tc} = \lambda$.

3 $t\bar{c}$ Production Through Vector-Boson Fusion

In this section we consider the reactions (see Fig. 1):

$$e^+e^- \rightarrow t\bar{c}\nu_e\bar{\nu}_e; \bar{t}c\nu_e\bar{\nu}_e, \quad e^+e^- \rightarrow t\bar{c}e^+e^-; \bar{t}ce^+e^-, \quad (13)$$

occurring via W^+W^- or ZZ fusion, which should be accessible to the Next generation of e^+e^- Linear Colliders (NLC) currently being envisaged [1]. We will see that these processes are very sensitive to FC currents [10].

An extremely interesting feature of the reactions in (13) is that at c.m. energies of TeV and above, the corresponding cross-sections can be much larger than the ones for the simple s -channel reactions in Model III: $e^+e^- \rightarrow t\bar{c}$ (see [6]) and $e^+e^- \rightarrow \mathcal{H}A \rightarrow t\bar{c}f\bar{f}; \bar{t}c\bar{c}$ (see [9]). For example, we find that $\sigma^{\nu\bar{\nu}tc} \equiv \sigma(e^+e^- \rightarrow t\bar{c}\nu_e\bar{\nu}_e + \bar{t}c\nu_e\bar{\nu}_e)$ is about two orders of magnitude larger than $\sigma(e^+e^- \rightarrow t\bar{c} + \bar{t}c)$ over a large region of parameter space, while $\sigma^{e\bar{e}tc} \equiv \sigma(e^+e^- \rightarrow t\bar{c}e^+e^- + \bar{t}ce^+e^-)$ is about one order of magnitude bigger than $\sigma(e^+e^- \rightarrow t\bar{c} + \bar{t}c)$. The crucial difference (and therefore interesting) feature of the VV fusion reactions is that, being a t -channel fusion process, the corresponding cross-sections *grow* with the c.m. energy of the collider. On the other hand, the “simple” s -channel reactions mentioned above *drop* like $1/s$. Thus, even if no $t\bar{c}$ events are detected at $\sqrt{s} = 500$ GeV via $e^+e^- \rightarrow t\bar{c}; \bar{t}c f\bar{f}; \bar{t}c\bar{c}$, there is still a strong motivation to look for a signature of (13) especially at somewhat higher energies.

In exploring the reactions $e^+e^- \rightarrow t\bar{c}\nu_e\bar{\nu}_e, \bar{t}ce^+e^-$ we will use the effective vector boson approximation (EVBA) [11]. Recall that this is the analog of the equivalent photon approximation

in QED which allows the colliding W 's or Z 's to be treated as on-shell particles. The salient features of the reactions in (13) are then well approximated by the simpler fusion reactions:

$$W^+W^-, ZZ \rightarrow t\bar{c}, \bar{t}c. \quad (14)$$

The corresponding cross sections for the reactions in (13) can then be calculated by folding in the distribution functions $f_{h_V}^V$, for a vector boson V (W or Z) with helicity h_V .

The EVBA has been extensively studied in the production of a $t\bar{t}$ pair [12]. There is, however, a significant difference between fusion reactions leading to a $t\bar{c}$ final state, due primarily to the appreciable difference in the threshold of the two-reactions (which, in turn, is due to $m_t \gg m_c$). This has two consequences:

1. For $t\bar{c}$ the vector-boson energy fraction, $x = \sqrt{\hat{s}}/s$ (as usual \hat{s} is the c.m. energy squared in the VV c.m. frame and s the corresponding quantity in the e^+e^- c.m. frame), can drop below $x = 0.05$ near threshold, for $\sqrt{s} \gtrsim 800$ GeV. In this small- x range the distribution functions are overestimated within the leading log approximation [12, 13]. We will therefore use the distribution functions which retain higher orders in m_V^2/s , as given, for example, by Johnson *et. al.* [13].
2. For large $\sqrt{\hat{s}}$, the longitudinal polarization vector of V can be approximated by $\epsilon_0^\mu(k) \simeq k^\mu/m_V + \mathcal{O}(m_V/\sqrt{\hat{s}})$. In the production of a pair of heavy fermions (such as $t\bar{t}$) through VV fusion, the term k^μ/m_V gives rise to a contribution proportional to $(m_t/m_V)^4$ in the cross section; the subleading contributions, generated by the $\mathcal{O}(m_V/\sqrt{\hat{s}})$ remainder in $\epsilon_0^\mu(k)$, are suppressed by a factor of $\sim m_t^2/\hat{s}$. Thus $\hat{\sigma}(VV \rightarrow t\bar{t})$ is well approximated by taking only the longitudinal polarized V 's at the parton level reaction and assuming that $\hat{s} \gg m_V^2$ [12, 13]. In contrast, the approximation $\epsilon_0^\mu(k) \simeq k^\mu/m_V$ does not necessarily hold for the reaction $VV \rightarrow t\bar{c}$ for which $m_V^2/\hat{s} \approx m_V^2/m_t^2$ near threshold. In particular, we will show below that the cross-section for the reaction $VV \rightarrow \mathcal{H} \rightarrow t\bar{c}$ scales like $|\epsilon_{h_{V1}}^{V1} \cdot \epsilon_{h_{V2}}^{V2}|^2$. Thus, not only is the $(m_t/m_V)^4$ factor absent, but the contribution from the transversely polarized V 's is comparable to that of the longitudinal V 's near threshold. We will therefore include all polarizations for the vector bosons in our calculation of $\hat{\sigma}(VV \rightarrow \mathcal{H} \rightarrow t\bar{c})$.

It is interesting to note that while at tree-level, $\sigma^{etc} = 0$ in the SM, the parton level reaction $W^+W^- \rightarrow t\bar{c}$ can proceed at tree-level, via diagram a in Fig. 1. Note that the corresponding cross section is proportional to $(m_t/m_W)^4$ to leading order, and the usual replacement $\epsilon_0^\mu(k) \rightarrow k^\mu/m_W$ is appropriate. For collision of longitudinal W 's, $W_L^+W_L^- \rightarrow t\bar{c}$, within the SM, we obtain:

$$\hat{\sigma}_{\text{SM}} = \frac{N_c \pi \alpha^2}{4s_W^4 \hat{s}^2} \left(\frac{m_t}{m_W} \right)^4 \sum_{i,j=1}^3 V_{ti} V_{tj}^* V_{ci} V_{cj}^* \left\{ \left(\frac{1}{\Delta_t} - 1 \right) I_{ij}^2 + \left(2 - \frac{1}{\Delta_t} \right) \frac{I_{ij}^3}{m_t^2} - \frac{I_{ij}^4}{m_t^4} \right\}, \quad (15)$$

where i, j are family indices, $s_W \equiv \sin \theta_W$ and $N_c = 3$ is the color factor. $\Delta_t \equiv m_t^2/\hat{s}$ and I_{ij}^k are the two body phase-space integrals:

$$I_{ij}^k \equiv \int_{m_t^2 - \hat{s}}^0 \frac{x^k dx}{(x - m_{d_i}^2)(x - m_{d_j}^2)} . \quad (16)$$

In (15) we have set $m_c = 0$, however the three down quarks masses must be kept non-zero as the unitarity of the Cabibbo-Kobayashi-Maskawa (CKM) matrix implies that $\hat{\sigma}_{\text{SM}} = 0$ when $m_d = m_s = m_b$ (in particular, when $m_d = m_s = m_b = 0$). Numerically, $\hat{\sigma}_{\text{SM}}$ is found to be too small to be of experimental relevance as it suffers from a severe CKM suppression: $\sigma_{\text{SM}}^{\nu\nu tc} \equiv \sigma_{\text{SM}}(e^+e^- \rightarrow t\bar{c}\nu_e\bar{\nu}_e + \bar{t}c\nu_e\bar{\nu}_e) \approx 10^{-5} - 10^{-4}$ (fb) for $\sqrt{s} = 0.5 - 2$ TeV. We will hence forward neglect the SM contribution.

This is, therefore, a remarkable situation which allows for a unique test of the SM and, in particular of the SM's GIM mechanism. Even a very small number of $t\bar{c}\nu_e\bar{\nu}_e$ and/or $t\bar{c}e^+e^-$ detected at a NLC running with a yearly integrated luminosity of $\mathcal{L} \gtrsim 10^2$ [fb] $^{-1}$ [1], will unmistakably indicate new FC dynamics beyond the SM. In Model III event numbers in the range of a few $\times (10^2 - 10^3)$ for $t\bar{c}\nu_e\bar{\nu}_e$, and a few $\times (10^1 - 10^2)$ for $t\bar{c}e^+e^-$ are easily possible within the existing experimental constraints.

For Model III, $VV \rightarrow t\bar{c}$ proceeds at tree-level via the \hat{s} -channel neutral Higgs exchange of diagram b in Fig. 1. Neglecting the SM diagram, the corresponding parton-level cross-section $\hat{\sigma}_V \equiv \hat{\sigma}(V_{h_{V1}}^1 V_{h_{V2}}^2 \rightarrow t\bar{c})$ is given by [10]:

$$\begin{aligned} \hat{\sigma}_V &= \frac{(\sin 2\tilde{\alpha})^2 N_c \pi \alpha^2}{4\hat{s}^2 \beta_V s_W^4} \left(\frac{m_V}{m_W} \right)^4 |\epsilon_{h_{V1}}^{V1} \cdot \epsilon_{h_{V2}}^{V2}|^2 |\Pi_h - \Pi_H|^2 \times \\ &\quad m_t m_c \sqrt{a_+ a_-} (a_+ \lambda_R^2 + a_- \lambda_I^2) , \end{aligned} \quad (17)$$

where:

$$a_{\pm} = \hat{s} - (m_t \pm m_c)^2 , \quad \beta_{\ell} \equiv \sqrt{1 - 4m_{\ell}^2/\hat{s}} , \quad (18)$$

and:

$$\Pi_{\mathcal{H}} = \frac{1}{(\hat{s} - m_{\mathcal{H}}^2 + im_{\mathcal{H}}\Gamma_{\mathcal{H}})} . \quad (19)$$

Given the couplings of Model III, $\Gamma_{\mathcal{H}}$ (the width of \mathcal{H}) can be readily calculated [14]. The leading decay rates in this model are $\mathcal{H} \rightarrow b\bar{b}, t\bar{t}, ZZ, W^+W^-$ and $t\bar{c}, c\bar{t}$. When kinematically allowed, we include all these contributions in calculating the above cross-sections. For definiteness, we will present our numerical results for $\tilde{\alpha} = \pi/4$.⁵ We will also ignore CP violation and take $\lambda_I = 0$ and $\lambda = \lambda_R$. In calculating the cross sections we first vary the mass of the lighter scalar h in the range $100 \text{ GeV} < m_h < 1 \text{ TeV}$, while holding fixed the mass of the heavy scalar H at $m_H = 1 \text{ TeV}$. We will later discuss the case $m_h \sim m_H$.

⁵As will be shown later, the VV fusion cross-sections in (13) reach their maxima at $\tilde{\alpha} \simeq \pi/6$ which is larger by a factor of ~ 1.5 than their value at $\tilde{\alpha} = \pi/4$; as indicated previously the cross sections vanish when $\tilde{\alpha} = 0, \pi/2$.

Due to the orthogonality properties of the V^1 and V^2 polarization vectors, there is no interference between the transverse and the longitudinal polarizations. Note that $|\epsilon_{\pm}^{V^1} \cdot \epsilon_{\mp}^{V^2}|^2 = 0$, $|\epsilon_{\pm}^{V^1} \cdot \epsilon_{\pm}^{V^2}|^2 = 1$, and $|\epsilon_0^{V^1} \cdot \epsilon_0^{V^2}|^2 = (1 + \beta_V^2)^2 / (1 - \beta_V^2)^2$ which grows with \hat{s} . However, we can see from (17), that $\hat{\sigma}_V(m_{\mathcal{H}}^2/\hat{s} \rightarrow 0) \rightarrow 0$ ensuring unitarity of the hard cross-section. In general, the transverse distribution functions are bigger than the longitudinal ones for $x \gtrsim 0.1$ [12, 13]. Therefore, the relative smallness of the transverse hard cross-section compared to the longitudinal one is partly compensated for in the full cross-section. In particular, we find that the contribution from the transversely polarized W 's(Z 's) constitutes up to 25% (35%) of the corresponding total cross-section $\sigma^{\nu\nu tc}(\sigma^{eetc})$.

It is evident from (17) that $\hat{\sigma}_W \rightarrow \hat{\sigma}_Z$ for $m_W \rightarrow m_Z$. The main difference between $\sigma^{\nu\nu tc}$ and σ^{eetc} then arises from the dissimilarity between the distribution functions for W and Z bosons. In particular, disregarding the subleading transverse parts of the WW and the ZZ cross-sections, the relative strength between the W and the Z longitudinal distribution functions is given by [13]:

$$f_0^Z = \frac{2}{c_W^2} \left(2s_W^4 - s_W^2 + \frac{1}{4} \right) f_0^W \approx \frac{1}{3} f_0^W. \quad (20)$$

Therefore, since the dominant contributions to the cross-sections $\sigma^{\nu\nu tc}$ and σ^{eetc} are produced by longitudinal W 's and Z 's, σ^{eetc} is expected to be smaller by about one order of magnitude than $\sigma^{\nu\nu tc}$, which is indeed what we find. We will thus only present numerical results for $\sigma^{\nu\nu tc}$, keeping in mind that σ^{eetc} exhibits the same behavior though suppressed by an order of magnitude.

Fig. 2 shows the dependence of the scaled cross-section $\sigma^{\nu\nu tc}/\lambda^2$ on the mass of the light Higgs m_h for four values of s .⁶ The cross-section peaks at $m_h \simeq 250$ GeV and drops as the mass of the light Higgs approaches that of the heavy Higgs due to the ‘‘GIM-like’’ cancellation present in the scalar sector (which is only partly effective when $\tilde{\alpha} \neq \pi/4$). Nonetheless, as will be shown below, $\sigma^{\nu\nu tc}/\lambda^2$ can stay at the fb level even for $m_h = m_H$. When $\sqrt{s} = 2$ TeV the cross-section is about 5 fb for $\lambda = 1$ and $m_h \approx 250$ GeV.⁷ It is therefore evident from Fig. 2 that at an NLC running at energies of $\sqrt{s} \gtrsim 1$ TeV and an integrated luminosity of the order of $\mathcal{L} \gtrsim 10^2$ [fb]⁻¹, Model III (with $\lambda = 1$) predicts hundreds and up to thousands of $t\bar{c}\nu_e\bar{\nu}_e$ events and several tens to hundreds of $t\bar{c}e^+e^-$ events. For example, with $\sqrt{s} = 1.5$ TeV, $\mathcal{L} = 500$ [fb]⁻¹ [1], and $m_h \approx 250$ GeV, $\lambda = 1$, the cross-section $\sigma^{\nu\nu tc}(\sigma^{eetc})$ would yield about 2000(200) such events. Note also that even with $m_h \approx 500$ GeV, this projected luminosity will still yield hundreds of $t\bar{c}\nu_e\bar{\nu}_e$ events and tens of $t\bar{c}e^+e^-$ events at $\sqrt{s} = 1.5$ TeV. The corresponding SM prediction yields, as shown above, essentially zero events.

The choice $\tilde{\alpha} = \pi/4$ is special in the sense that for this value the GIM-like cancellation mentioned above is most effective, however, it does not correspond to the maximum of the production rates. In Fig. 3 we show the dependence of $\sigma^{\nu\nu tc}/\lambda^2$ on $(\sin \tilde{\alpha})^2$ for $m_h = 250$

⁶The scaled cross-section, $\sigma^{\nu\nu tc}/\lambda^2$, has a residual mild dependence on λ through its dependence on Γ_h .

⁷The cross-section is $\propto \lambda^2$ so that even a moderate change of λ , say by a factor of three, can increase or decrease the cross-section by one order of magnitude.

GeV, $\sqrt{s} = 1$ TeV and for two possible values of m_H , $m_H = 250$ GeV and $m_H = 1$ TeV. The same behavior is observed for any value of s in the range 0.5–2 TeV. We see that for $m_H = 1$ TeV, which represents the case of large splitting between the two neutral Higgs particles, $\sigma^{\nu\bar{\nu}tc}(\pi/14 \lesssim \tilde{\alpha} \lesssim \pi/4) > \sigma^{\nu\bar{\nu}tc}(\tilde{\alpha} = \pi/4)$. Moreover, even for $(m_H - m_h) \approx 0$, $\sigma^{\nu\bar{\nu}tc} \gtrsim 1$ fb is still possible for $0.02 \lesssim (\sin \tilde{\alpha})^2 \lesssim 0.22$ and $0.78 \lesssim (\sin \tilde{\alpha})^2 \lesssim 0.98$. In fact, our analysis shows that, with moderate restrictions on $\tilde{\alpha}$, $\sigma^{\nu\bar{\nu}tc}$ remains well above the fb level for $\sqrt{s} \gtrsim 1$ TeV as long as one of the neutral Higgs particles is kept within $200 \text{ GeV} \lesssim m_H \lesssim 400 \text{ GeV}$, while the mass of the other Higgs can take practically any value between $100 \text{ GeV} - 1000 \text{ GeV}$. Moreover, note that as $\tilde{\alpha}$ drops below $\pi/6$ the cross-section becomes less sensitive to the heavy Higgs mass. For example, we find that with $\tilde{\alpha} \approx \pi/27$ (which may represent the case of a small $\tilde{\alpha}$) and for $\sqrt{s} = 1$ TeV, $\sigma^{\nu\bar{\nu}tc} \approx 1$ fb regardless of the heavy Higgs mass (i.e., $m_H = 250 - 1000$ GeV) and as one goes to $\sqrt{s} > 1$ TeV, $\sigma^{\nu\bar{\nu}tc}$ becomes even bigger. It is therefore clear that the FC effect being investigated in this section remains very interesting within a large portion of the free parameter space of the Higgs sector in Model III.

Before ending this section we wish to comment further on the comparison between the cross-section $\sigma(e^+e^- \rightarrow t\bar{c})$ discussed in [6] and the WW annihilation cross-section $\sigma^{\nu\bar{\nu}tc}$ within Model III. To do so, for convenience, we normalize the cross sections to the $\mu^+\mu^-$ cross-section:

$$R^{\nu\bar{\nu}tc} \equiv \frac{\sigma(e^+e^- \rightarrow t\bar{c}\nu_e\bar{\nu}_e + \bar{t}c\nu_e\bar{\nu}_e)}{\sigma(e^+e^- \rightarrow \gamma \rightarrow \mu^+\mu^-)}, \quad R^{tc} \equiv \frac{\sigma(e^+e^- \rightarrow t\bar{c} + \bar{t}c)}{\sigma(e^+e^- \rightarrow \gamma \rightarrow \mu^+\mu^-)}. \quad (21)$$

Note that while $R^{\nu\bar{\nu}tc}$ scales as λ^2 , R^{tc} is proportional to λ^4 . It was shown in [6] that R^{tc}/λ^4 can reach 10^{-5} for a light Higgs mass around 200 GeV and c.m. energy of $\sqrt{s} = 500$ GeV. As the c.m. energy is increased R^{tc}/λ^4 stays fixed at the 10^{-5} level due to the $\sim 1/s$ behavior of $\sigma(e^+e^- \rightarrow t\bar{c} + \bar{t}c)$ with one loop FC Higgs exchanges.

In Figs. 4 and 5 we have plotted $R^{\nu\bar{\nu}tc}/\lambda^2$ as a function of m_h and \sqrt{s} , respectively. We see that for $m_h \approx 250$ GeV and a c.m. energy of $\sqrt{s} = 500$ GeV $R^{\nu\bar{\nu}tc}/\lambda^2$ peaks at around 10^{-3} , two orders of magnitude above R^{tc}/λ^4 . We therefore expect the number of $t\bar{c}\nu_e\bar{\nu}_e$ events in the NLC to be bigger by about two orders of magnitude than the number of $t\bar{c}$ events. Moreover, while the cross-section for producing a pair of $t\bar{c}$ sharply drops as \sqrt{s} is increased, the WW fusion cross-section, $\sigma^{\nu\bar{\nu}tc}$ grows with s . In particular, Figs. 4 and 5 show that for $200 \text{ GeV} \lesssim m_h \lesssim 400 \text{ GeV}$, $R^{\nu\bar{\nu}tc}/\lambda^2 \sim 10^{-2}$ for $\sqrt{s} \sim 1$ TeV and $R^{\nu\bar{\nu}tc}/\lambda^2 \sim 10^{-1}$ for $\sqrt{s} \sim 2$ TeV.

4 $e^+e^- \rightarrow t\bar{c}\nu_e\bar{\nu}_e$ vs. $e^+e^- \rightarrow t\bar{t}\nu_e\bar{\nu}_e$ and Background Considerations

In order to give the reader a qualitative feel for the effectiveness of the $t\bar{c}\nu_e\bar{\nu}_e$ production rate it is instructive to compare it, in Model III, to the production rate of the “normal” $e^+e^- \rightarrow t\bar{t}\nu_e\bar{\nu}_e$. We recall that $\sigma^{\nu\bar{\nu}tt} \equiv \sigma(e^+e^- \rightarrow W^+W^-\nu_e\bar{\nu}_e \rightarrow t\bar{t}\nu_e\bar{\nu}_e)$ is dominated by collisions of two longitudinal W ’s at the parton level [12]. The reaction $W^+W^- \rightarrow t\bar{t}$ can proceed through

the t -channel b quark exchange and the s -channel γ, Z, h and H exchanges (the diagrammatic description can be found in [12, 15]).

The helicity amplitudes $\mathcal{A}_{\eta=\bar{\eta}}, \mathcal{A}_{\eta=-\bar{\eta}}$ (η and $\bar{\eta}$ denote the helicities of the t and \bar{t} quarks, respectively) for $W_L^+ W_L^- \rightarrow t\bar{t}$, including all the contributing diagrams, are given by:

$$\mathcal{A}_{\eta=\bar{\eta}} = \frac{\pi\alpha}{s_W^2} \frac{m_t \sqrt{\hat{s}}}{m_W^2} \left(\left[\frac{(1 + \beta_t^2) \cos \theta - 2\beta_t}{1 + \beta_t^2 - 2\beta_t \cos \theta} \right] - \sum_{\mathcal{H}=h,H} \sqrt{2} c_{\mathcal{H}} (a_{\mathcal{H}} \beta_t - i\eta b_{\mathcal{H}}) \Pi_{\mathcal{H}} \right), \quad (22)$$

$$\mathcal{A}_{\eta=-\bar{\eta}} = \frac{2\pi\alpha}{s_W^2} \frac{m_t^2}{m_W^2} \left(\frac{\eta + \beta_t}{1 + \beta_t^2 - 2\beta_t \cos \theta} \right) \sin \theta, \quad (23)$$

where θ is the c.m. scattering angle and $a_{\mathcal{H}}, b_{\mathcal{H}}$ and $c_{\mathcal{H}}$ are given in (11), (12) and (8). In the SM limit $\tilde{\alpha} = -\pi/4$ and $\lambda_R, \lambda_I = 0$, the hard cross-section for $W_L^+ W_L^- \rightarrow t\bar{t}$, obtained from (22) and (23) agrees with the one obtained by Eboli *et. al.* in [12].

We give below only the “non-standard” parts $\hat{\sigma}_{hh}, \hat{\sigma}_{HH}, \hat{\sigma}_{hH}, \hat{\sigma}_{bh}$ and $\hat{\sigma}_{bH}$:⁸

$$\hat{\sigma}_{hh} = \mathcal{G}_t (\sin \tilde{\alpha})^2 |\Pi_h|^2 \left(\beta_t^2 a_h^2 + b_h^2 \right), \quad (24)$$

$$\hat{\sigma}_{HH} = \mathcal{G}_t (\cos \tilde{\alpha})^2 |\Pi_H|^2 \left(\beta_t^2 a_H^2 + b_H^2 \right), \quad (25)$$

$$\hat{\sigma}_{hH} = -\mathcal{G}_t \sin 2\tilde{\alpha} \text{Re}(\Pi_h \Pi_H^*) \left(\beta_t^2 a_h a_H + b_h b_H \right), \quad (26)$$

$$\hat{\sigma}_{bh} = \mathcal{G}_t \sin \tilde{\alpha} a_h (1 - \Delta_h) |\Pi_h|^2 \left[\frac{(1 - \beta_t^2)^2}{2\beta_t} \Lambda - (1 + \beta_t^2) \right], \quad (27)$$

$$\hat{\sigma}_{bH} = -\mathcal{G}_t \cos \tilde{\alpha} a_H (1 - \Delta_H) |\Pi_H|^2 \left[\frac{(1 - \beta_t^2)^2}{2\beta_t} \Lambda - (1 + \beta_t^2) \right], \quad (28)$$

where $\hat{\sigma}_{ij}$, $i \neq j$ denotes the interference cross-section of the i and j intermediate states, and:

$$\mathcal{G}_t \equiv \frac{N_c \pi \alpha^2}{4s_W^4} \frac{m_t^2}{m_W^4} \beta_t, \quad \Lambda \equiv \ln \left(\frac{\beta_t + 1}{\beta_t - 1} \right). \quad (29)$$

In Fig. 6 we plot the ratio $R^{tc/tt} \equiv \sigma^{\nu tc} / \sigma^{\nu tt}$ within Model III for $\lambda = 1$,⁹ $\tilde{\alpha} = \pi/4$ and $m_H = 1$ TeV as a function of the light Higgs mass m_h and for $\sqrt{s} = 0.5, 1, 1.5, 2$ TeV. $\sigma^{\nu tt}$ depends very weakly on m_h , with a small peak at $m_h \simeq 400$ GeV which fades as \sqrt{s} grows. Therefore, $R^{tc/tt}$ peaks with $\sigma^{\nu tc}$ at $m_h \simeq 250$ GeV. We can see from Fig. 6 that for $\sqrt{s} = 0.5$ TeV and in the range $200 \text{ GeV} \lesssim m_h \lesssim 400 \text{ GeV}$, $R^{tc/tt} > 1$. In particular, for $m_h \approx 250$ GeV, $\sigma^{\nu tc}$ can become almost two orders of magnitude larger than $\sigma^{\nu tt}$. As \sqrt{s} grows, $R^{tc/tt}$ drops. In the range $200 \text{ GeV} \lesssim m_h \lesssim 400 \text{ GeV}$, we find that for $\sqrt{s} = 1$ TeV, $R^{tc/tt} > 0.1$, while for $\sqrt{s} = 1.5 - 2$ TeV, $0.01 \lesssim R^{tc/tt} \lesssim 0.1$.

⁸The SM-like parts can be extracted from the paper by Eboli *et. al.* in [12] by changing the appropriate quantum numbers of the final state fermions.

⁹Recall that we have assumed for simplicity that $\lambda_{tt} = \lambda_{tc} = \lambda$.

The dependence of $\sigma^{\nu\nu tt}$ on λ is significant only near its peak (at $m_h \sim 400$ GeV); for $200 \text{ GeV} \lesssim m_h \lesssim 400 \text{ GeV}$, where $R^{tc/tt}$ acquires its largest values, $R^{tc/tt}$ roughly scales as λ^2 . Thus, again a mild change in λ , can alter $R^{tc/tt}$ appreciably. Hence, within Model III, with m_h in the few-hundred GeV range, it is possible to observe comparable production rates for the $t\bar{c}\nu_e\bar{\nu}_e$ and $t\bar{t}\nu_e\bar{\nu}_e$ even at a NLC running at a TeV range c.m. energies.

We have not done any serious study on the issue of backgrounds. For example, $\nu_e\bar{\nu}_e W^+ W^-$ is expected to be about an order of magnitude bigger than $\nu_e\bar{\nu}_e t\bar{t}$ and therefore could be of concern. However, we remark that the NLC literature suggests that detection of t (or \bar{t}) via the main mode $t \rightarrow bqq'$ (i.e., 3-jet events) with the constraint $m_{\text{jet1}} + m_{\text{jet2}} = m_W$ can be achieved with a relatively high efficiency [16]. The $\nu\nu WW$ cross-section also has distinctive constraints on it that, along with the rather clean t detection, are expected to be very effective in separating it from $\nu\nu tt$ or $\nu\nu tc$ final states. In the case of the $\nu_e\bar{\nu}_e t\bar{c}$ final state, in addition to the top-quark detection via, for example, the 3-jet mode, the other (charm) jet is rather unique and should stand out as essentially a light quark jet, i.e., the event should look like a *single* top quark event. Therefore, it will be difficult to fake a $t\bar{c}$ event with a $t\bar{t}$ or WW event.

5 The Reaction $f\bar{f}' \rightarrow Vt\bar{c}$

In this section we explore the possibility of observing a signature of a $Zt\bar{c}$ final state (and its conjugate one) at the NLC. Within Model III, the reaction $f\bar{f}' \rightarrow Vt\bar{c}$ ($V = Z, W^+$ or W^- depending on the quantum numbers of the $f\bar{f}'$ initial state) proceeds at tree-level via the Feynman diagram depicted in Fig. 7. Of course, disregarding the incoming $f\bar{f}'$ fermions, this reaction is directly related to the sub-process $VV \rightarrow \mathcal{H} \rightarrow t\bar{c}$. We can therefore express the cross-section $\sigma(f\bar{f}' \rightarrow Vt\bar{c})$ in terms of the hard cross-section $\hat{\sigma}_V$ given in (17):

$$\sigma(f\bar{f}' \rightarrow Vt\bar{c}) = \frac{\alpha}{6\pi(\sin 2\theta_W)^2} \Delta_V \Pi_V^2 \left\{ \left[a_L^{f(V)} \right]^2 + \left[a_R^{f(V)} \right]^2 \right\} \times \int_1^{(\Delta_t^{-1/2} - \zeta_V)^2} dz \omega_1 \omega_2 \frac{\omega_1^2 + 12\Delta_V}{\omega_2^2 + 12\zeta_V^4} \sum_{h_{V1}, h_{V2}} \hat{\sigma}_V|_{\hat{s}=m_t^2 z} . \quad (30)$$

Here $\Delta_\ell \equiv m_\ell^2/s$ (s being the c.m. energy of the colliding $f\bar{f}'$ fermions) and $\Pi_V = (1 - \Delta_V)^{-1}$. Also $\zeta_\ell \equiv m_\ell/m_t$ and ω_1, ω_2 are function of z given by:

$$\omega_1 = \sqrt{\left(1 - (\sqrt{\Delta_V} + \sqrt{\Delta_t z})\right) \left(1 - (\sqrt{\Delta_V} - \sqrt{\Delta_t z})\right)} , \quad (31)$$

$$\omega_2 = z\sqrt{1 - 4z^{-1}\zeta_V^2} , \quad (32)$$

and we have defined the $Vf\bar{f}'$ interaction lagrangian as:

$$\mathcal{L}_{V\mu f f'} \equiv \frac{g_W}{c_W} V_\mu \gamma_\mu \bar{f}' \left(a_L^{f(V)} L + a_R^{f(V)} R \right) f , \quad (33)$$

where $L(R) = (1 \mp \gamma_5)/2$.

The formula given in (30) is general and can be applied, for example, for calculating the sub-process cross-sections $u\bar{u}, d\bar{d} \rightarrow Zt\bar{c}$ and $u\bar{d}; \bar{u}d \rightarrow W^+t\bar{c}; W^-t\bar{c}$ relevant for hadron colliders. Here we wish to concentrate only on the cross-section $\sigma^{Ztc} \equiv \sigma(e^+e^- \rightarrow Zt\bar{c} + Z\bar{t}c)$ relevant for the NLC and for which $V = Z$, $f = e^-$, $\bar{f}' = e^+$ and $a_L^{e(Z)} = 1/2 - s_W^2$, $a_R^{e(Z)} = s_W^2$. The production of a real Higgs boson and a Z boson via $e^+e^- \rightarrow Z \rightarrow Z\mathcal{H}$ followed by the \mathcal{H} decay $\mathcal{H} \rightarrow t\bar{c}$ was investigated in [9]. This is of relevance whenever there is sufficient energy to produce a real $Z\mathcal{H}$ pair and $m_{\mathcal{H}} > m_t + m_c$, then:

$$\sigma(e^+e^- \rightarrow Z\mathcal{H} \rightarrow Zt\bar{c} + Z\bar{t}c) \approx \sigma(e^+e^- \rightarrow Z \rightarrow Z\mathcal{H}) \times \text{Br}(\mathcal{H} \rightarrow t\bar{c} + \bar{t}c) . \quad (34)$$

Here we will extend the analysis performed in [9] by including both neutral Higgs particles, produced either as real or virtual particles.

In Fig. 8 we plot σ^{Ztc}/λ^2 as a function of the light Higgs mass, m_h , for various values of \sqrt{s} , and in Fig. 9, σ^{Ztc}/λ^2 as a function of s for various values of m_h ($m_H = 1$ and $\tilde{\alpha} = \pi/4$ are kept fixed). We see that there is a significant difference between σ^{Ztc} and $\sigma^{\nu\nu tc}, \sigma^{eetc}$; the former drops with s (as expected for an s-channel process) while the latter increase with s . Therefore, a search for a Ztc signature will be most effective at lower energies. In particular, we find that σ^{Ztc}/λ^2 peaks when the c.m. energy is a few tens of GeV above the threshold for producing a real hZ pair. At $\sqrt{s} = 500$ GeV and for $200 \text{ GeV} \lesssim m_h \lesssim 350 \text{ GeV}$, $\sigma^{Ztc}/\lambda^2 \gtrsim 0.2 \text{ fb}$ and peaks for $m_h \approx 250 \text{ GeV}$ at $\sim 0.6 \text{ fb}$. In this range h is produced on-shell and then decays to $t\bar{c}$.

Apart from the overall factor of $(\sin 2\tilde{\alpha})^2$ in the cross-section (from the $VV \rightarrow \mathcal{H} \rightarrow t\bar{c}$ matrix element), there is an additional strong dependence on $\tilde{\alpha}$ coming from $\text{Br}(h \rightarrow t\bar{c} + \bar{t}c)$. This quantity also generates a strong suppression (for $\tilde{\alpha} = \pi/4$, $\text{Br}(h \rightarrow t\bar{c} + \bar{t}c) \approx 10^{-2}$) since h decays mainly into W pairs: $\text{Br}(h \rightarrow W^+W^-) \sim 1$ for $\tilde{\alpha} = \pi/4$ and $2m_t > m_h > 2m_W$ and $\text{Br}(h \rightarrow W^+W^-) \sim 0.7 \gg \text{Br}(h \rightarrow t\bar{t})$ when $m_h > 2m_t$. In contrast, within the SM $\text{Br}(h \rightarrow W^+W^-) \sim \text{Br}(h \rightarrow t\bar{t}) \sim 0.5$ for $m_h > 2m_t$.

Similar to the VV fusion case, when there is large splitting between the masses of the two neutral scalars (i.e., $m_H = 1 \text{ TeV}$), σ^{Ztc}/λ^2 is maximized for $\tilde{\alpha} \approx \pi/6$. In Fig. 10 we plot σ^{Ztc}/λ^2 as a function of $(\sin \tilde{\alpha})^2$ for $\sqrt{s} = 500 \text{ GeV}$, $m_h = 250 \text{ GeV}$ and $m_H = 250, 1000 \text{ GeV}$.¹⁰ As can be seen by comparing Fig. 3 with Fig. 10, σ^{Ztc} and $\sigma^{\nu\nu tc}$ exhibit the same dependence on $\tilde{\alpha}$ since both reactions are governed by the $VV - \mathcal{H} - tc$ amplitude; we again find that for $m_H = 1 \text{ TeV}$, $\sigma^{Ztc}(\pi/14 \lesssim \tilde{\alpha} \lesssim \pi/4) > \sigma^{Ztc}(\tilde{\alpha} = \pi/4)$. When $m_H \approx m_h \approx 250 \text{ GeV}$, $\sigma^{Ztc} \gtrsim 0.2 \text{ fb}$ is still possible for $0.02 \lesssim (\sin \tilde{\alpha})^2 \lesssim 0.28$ and $0.75 \lesssim (\sin \tilde{\alpha})^2 \lesssim 0.98$.

We thus conclude that at an NLC running at $\sqrt{s} = 500 \text{ GeV}$ and a yearly integrated luminosity of $\mathcal{L} \gtrsim 10^2 [\text{fb}]^{-1}$ we can expect several tens and up to hundred such Ztc raw events for $200 \text{ GeV} \lesssim m_h \lesssim 350 \text{ GeV}$ (the number depends on $\tilde{\alpha}$ but is insensitive to m_H). However, unlike the $\nu\nu tc$ and the $eetc$ signals which form a relatively clean signature (especially at higher energies, i.e. $\sqrt{s} \gtrsim 1 \text{ TeV}$, where there is practically no competing process that can produce a pair of $t\bar{c}$), the $Zt\bar{c}$ final state may suffer from severe background problems if scalar FC interactions are indeed present. For example, assuming that a $t\bar{c}$ pair can be detected with

¹⁰Here also, the same behavior as a function of $(\sin \tilde{\alpha})^2$ occurs for higher energies.

some efficiency factor, still, the production rate of a pair of $\mathcal{H}A$ via $e^+e^- \rightarrow Z \rightarrow \mathcal{H}A$ followed by the decays $A \rightarrow t\bar{c}$ and $\mathcal{H} \rightarrow f\bar{f}$ (recall that $\mathcal{H} = h$ or H and f stands for a fermion) may well overwhelm that of $e^+e^- \rightarrow Z \rightarrow Zt\bar{c}$.

6 The Rare Top Decays $t \rightarrow W^+W^-c$, $t \rightarrow ZZc$

Finally we wish to discuss the two rare decays $t \rightarrow W^+W^-c$ and $t \rightarrow ZZc$. The latter being possible only if $m_t > 2m_Z + m_c$ (which is still allowed by the data). Within the SM these decay channels are vanishingly small. For the first one, $t \rightarrow W^+W^-c$, even though a tree-level decay in the SM (i.e., the tree-level diagram is the same as the one depicted in Fig. 1a without the electron-neutrino fermionic lines), suffers from the same severe CKM suppression which appears in the subprocess $W^+W^- \rightarrow t\bar{c}$ considered before. Typically, one finds $\text{Br}(t \rightarrow W^+W^-c) \approx 10^{-13} - 10^{-12}$ for $160 \text{ GeV} \lesssim m_t \lesssim 200 \text{ GeV}$ [17, 18]. For the second decay $t \rightarrow ZZc$, the branching ratio is even smaller since it occurs only at one loop and in addition it is also GIM suppressed.

The situation is completely different in Model III where both decay modes can occur at the tree-level through the FC Higgs exchange of Fig. 1b (without the leptonic lines) and the CKM factors are absent. These decays are thus related to the fusion reactions, $WW, ZZ \rightarrow t\bar{c}$, by crossing symmetry. Therefore, in terms of the hard cross-section given in (17):

$$\Gamma_{VV} \equiv \Gamma(t \rightarrow VVc) = \frac{m_t^3}{32N_c\pi^2} \int_{4\zeta_V^2}^{(1-\zeta_c)^2} dz \, z(z - 4\zeta_V^2) \sum_{h_{V1}, h_{V2}} \hat{\sigma}_V|_{\hat{s}=m_t^2 z} . \quad (35)$$

The scaled branching-ratio $\text{Br}(t \rightarrow W^+W^-c)/\lambda^2$ is given in Fig. 11 as a function of the light Higgs mass and for $m_t = 170, 180$ and 190 GeV . Also, in Table 1 we present the branching-ratios for both $t \rightarrow W^+W^-c$ and $t \rightarrow ZZc$ where we focus on the range $m_t - 25 \text{ GeV} < m_h < m_t + 25 \text{ GeV}$ (keeping $m_h > 2m_W$). We see that $\text{Br}(t \rightarrow W^+W^-c)/\lambda^2$ is largest for $2m_W \lesssim m_h \lesssim m_t$ and drops rapidly when $m_h < 2m_W$ or $m_h > 200 \text{ GeV}$. The reason is that when $m_h < 2m_W$ or $m_h > m_t$, the decay $t \rightarrow W^+W^-c$ is a genuine 3-body decay. Thus, it suffers a suppression factor $\sim \text{Br}(t \rightarrow W^+W^-c)/\text{Br}(t \rightarrow hc)$ compared to the essentially 2-body case, $t \rightarrow hc$, which is relevant for the window, $2m_W \lesssim m_h \lesssim m_t$. $\text{Br}(t \rightarrow W^+W^-c)/\lambda^2$ is typically a few times 10^{-8} for $m_h \gtrsim m_t$ and can reach $\sim 10^{-6}$ in the $m_h \lesssim 2m_W$ region. For a wide range of m_h , i.e. from about 50 GeV to about 300 GeV , $\text{Br}(t \rightarrow W^+W^-c)/\lambda^2$ is 3–4 orders of magnitude larger than the SM prediction.

For optimal values of m_h , lying in the very narrow window, $2m_W \lesssim m_h \lesssim m_t$, we find that $\text{Br}(t \rightarrow W^+W^-c)/\lambda^2$ can reach the 10^{-5} – 10^{-4} level. In this region the t -quark decays to an on-shell Higgs boson followed by the decay $h \rightarrow W^+W^-$. Note that the process $t \rightarrow ch$ studied in [7] is related to the reaction $t \rightarrow W^+W^-c$ under discussion here. In the region $2m_W \lesssim m_h \lesssim m_t$ the decay width satisfies $\Gamma_{WW} \approx \Gamma(t \rightarrow ch) \times \text{Br}(h \rightarrow W^+W^-)$. Note, however, that the analytical results of [7] correspond to the choice $\tilde{\alpha} \rightarrow 0$ and in this special case Higgs decays to WW, ZZ are suppressed at tree level even when $m_h > 2m_W$. In the

present paper we use the more generic value $\tilde{\alpha} = \pi/4$ in which case $h \rightarrow WW$ becomes the dominant h decay.

Concerning $t \rightarrow ZZc$, the branching ratio is typically $\sim 10^{-5}$ for $2m_Z + m_c < m_t < 200$ GeV if again m_h lies in the very narrow window $2m_Z \lesssim m_h \lesssim m_t$. Also, both decays are very sensitive to m_t . In Fig. 12 we have plotted $\text{Br}(t \rightarrow W^+W^-c)/\lambda^2$ and $\text{Br}(t \rightarrow ZZc)/\lambda^2$ as a function of m_t holding fixed the mass of the heavy Higgs boson at $m_H = 1$ TeV and taking $m_h = 170$ and 185 GeV. We see that a ~ 10 GeV shift in m_t can easily generate an order of magnitude change in the branching ratios. For some possible values of m_h in the range $150 \text{ GeV} \lesssim m_h \lesssim 200 \text{ GeV}$ it can even generate a change of several orders of magnitude.

7 Summary and outlook

In this paper, we have emphasized the importance of searching for the FC reactions $e^+e^- \rightarrow t\bar{c}\nu_e\bar{\nu}_e$, $e^+e^- \rightarrow t\bar{c}e^+e^-$ and $e^+e^- \rightarrow Zt\bar{c}$ in a high energy e^+e^- collider. These reactions are very sensitive indicators of physics beyond the SM with new FC couplings of the top quark. As an illustrative example we have considered the consequences of extending the scalar sector of the SM with a second scalar doublet such that new FC couplings occur at the tree-level. At $\sqrt{s} = 500$ GeV the production rates for the $Zt\bar{c}$ and $t\bar{c}\nu_e\bar{\nu}_e$ final states are comparable (several tens of raw events are expected). However, for c.m. energies at the TeV level and above, we found that within a large portion of the parameter space of the FC 2HDM, i.e. Model III, in a one year of running with a yearly integrated luminosity of $\mathcal{L} \gtrsim 100\text{--}500 \text{ [fb]}^{-1}$, these new FC couplings may give rise to several hundreds and up to a few thousands $t\bar{c}\nu_e\bar{\nu}_e$ events and tens to hundreds of $t\bar{c}e^+e^-$ events in the NLC. This will unambiguously indicate the existence of new physics.

We have shown that the comparison between $\sigma^{\nu\nu tc}$ and the “normal” $\sigma^{\nu\nu tt}$ comes out favorable in these models. The $t\bar{c}$ final state involved, is rather distinctive and, therefore, serious background problems for either the $t\bar{c}\nu_e\bar{\nu}_e$ or the $t\bar{c}e^+e^-$ signatures are not anticipated. Moreover, from the experimental point of view, it should be emphasized that although σ^{eetc} is found to be one order of magnitude smaller than $\sigma^{\nu\nu tc}$, the $t\bar{c}e^+e^-$ signature may be easier to detect as it does not have the missing energy associated with the two neutrinos in the $t\bar{c}\nu_e\bar{\nu}_e$ final state. Also, at $\sqrt{s} \gtrsim 1$ TeV, the $t\bar{c}\nu_e\bar{\nu}_e$ and $t\bar{c}e^+e^-$ signatures are to some extent unique, as other simple FC s -channel processes like $e^+e^- \rightarrow Z \rightarrow t\bar{c}$, $e^+e^- \rightarrow Z\mathcal{H} \rightarrow Zt\bar{c}$ and $e^+e^- \rightarrow A\mathcal{H} \rightarrow t\bar{t}c\bar{c}, t\bar{c}f\bar{f}$ tend to drop as $1/s$ and are therefore expected to yield much smaller production rates at an e^+e^- collider with $\sqrt{s} \gtrsim 1$ TeV.

We have also examined the two rare top decays $t \rightarrow W^+W^-c$ and $t \rightarrow ZZc$. We found that, within Model III, the branching ratios are many orders of magnitudes bigger than the SM ones. However, detection of such exotic signatures may not be possible at the NLC as it is expected to produce $\sim \text{few} \times 10^4$ $t\bar{t}$ pairs. However, if nature provides us with a scalar particle, h , with mass in the range $150 \text{ GeV} \lesssim m_h \lesssim 200 \text{ GeV}$ and with FC couplings to tc , then the LHC, which will be capable of producing $10^7 - 10^8$ $t\bar{t}$ pairs, will be able to detect those rare signatures of top decays.

We wish to end with the following remarks and outlook:

- Note that in our previous work, [10], we have used $m_H = 750$ GeV while here we have set the heavy Higgs mass to be $m_H = 1$ TeV. No significant difference between the two choices is observed.
- It is most likely that the Higgs particles, if at all present, will have been discovered by the time the NLC starts its first run. If indeed such a particle is detected with a mass of a few hundreds GeV, it will be extremely important to investigate the reactions $e^+e^- \rightarrow t\bar{c}\nu_e\bar{\nu}_e$ and $e^+e^- \rightarrow t\bar{c}e^+e^-$ in the NLC as they may serve as strong evidence for the existence of a nonminimal scalar sector with FC scalar couplings to fermions. In addition, since supersymmetry strongly disfavors an h heavier than ~ 150 GeV, the detection of a Higgs particle above this limit would drive the study of general extended scalar sector, not of a supersymmetric origin, and, in turn, this should encourage the study of FC effects such as the ones studied in this paper.
- The large FC effects in $e^+e^- \rightarrow t\bar{c}\nu_e\bar{\nu}_e$ and $e^+e^- \rightarrow t\bar{c}e^+e^-$ described above may serve as a “yardstick” for other, possibly large, FC effects in those same reactions. In this sense, a model independent analysis of the reactions $e^+e^- \rightarrow t\bar{c}\nu_e\bar{\nu}_e$ and $e^+e^- \rightarrow t\bar{c}e^+e^-$ can be very useful. This can proceed by either incorporating explicit phenomenological FC vertices of $Ztc, WWtc, ZZtc$ etc., or by considering new effective couplings (possibly right-handed) of the W boson to the top and a down-type quark which will affect Fig. 1a [19]. Note that the effects of an effective Ztc coupling, if at all measurable, will be directly probed in the reaction $e^+e^- \rightarrow Z \rightarrow t\bar{c}$ whose cross section is larger by a factor of $\sim (\alpha/\pi)^2$ (α being the fine structure constant) than the one for $t\bar{c}\nu_e\bar{\nu}_e$ through WW fusion. Therefore, if a vanishing production rate for $e^+e^- \rightarrow Z \rightarrow t\bar{c}$ is measured in a NLC with a c.m. energy around $\sqrt{s} = 500$ GeV, then the possibility of a significant Ztc coupling will be basically eliminated.
- The cross-sections for $e^+e^- \rightarrow t\bar{c}\nu_e\bar{\nu}_e$ and $e^+e^- \rightarrow t\bar{c}e^+e^-$ grow with the c.m. energy of the colliding fermions. Therefore, an analogous study, for the LHC, of production of tc pairs via VV fusion may be even more interesting. However, note that in the LHC, these type of reactions are likely to suffer from much worse background problems.

We will refer to some of these points in a later work.

Acknowledgments

We thank David Atwood, Keisuke Fujii, George Hou, Mark Sher and Daniel Wyler for discussions. We acknowledge partial support from U.S. Israel B.S.F. (G.E. and A.S.) and from the U.S. DOE contract numbers DE-AC02-76CH00016(BNL), DE-FG03-94ER40837(UCR). G.E. thanks the Israel Science Foundation and the Fund for the Promotion of Research at the Technion for partial support.

Note Added. After completion of this manuscript, which is an extension of our previous work [10], we became aware of a very recent work [20] where (among other things) an exact calculation for the reaction $e^+e^- \rightarrow t\bar{c}\nu_e\bar{\nu}_e$ is reported. The difference with the effective vector boson approximation used here appears to be at the order of 10% in the range $200 \text{ GeV} < m_h < 400 \text{ GeV}$ and $1 \text{ TeV} < \sqrt{s} < 2 \text{ TeV}$. For $m_H \gtrsim 400 \text{ GeV}$ and $1 \text{ TeV} < \sqrt{s} < 2 \text{ TeV}$ the difference can be at the order of 30% or so. In general the difference diminishes as \sqrt{s} decreases.

References

- [1] Proceedings of the Workshop on Physics and Experiments with Linear e^+e^- Colliders, eds. F. Harris S. Olsen, S. Pakvasa and X. Tata, World Scientific, Singapore, 1993; Proceedings of the Workshop on Physics and Experiments with Linear e^+e^- Colliders, eds. A. Miyamoto and Y. Fujii, World Scientific, Singapore, 1996.
- [2] M. Luke and M.J. Savage, Phys. Lett. **B307**, 387 (1993).
- [3] S. Glashow and S. Weinberg, Phys. Rev. **D15**, 1958 (1977).
- [4] T.P. Cheng and M. Sher, Phys. Rev. **D35**, 3484 (1987); M. Sher and Y. Yuan, Phys. Rev. **D44**, 1461 (1991).
- [5] D. Atwood, L. Reina and A. Soni, Phys. Rev. **D55**, 3156 (1997).
- [6] D. Atwood L. Reina and A. Soni, Phys. Rev. **D53**, 1199 (1996).
- [7] M.J. Savage, Phys. Lett. **B266**, 135 (1991); W.S. Hou, Phys. Lett. **B296**, 179 (1992); L.J. Hall and S. Weinberg, Phys. Rev. **D48**, R979 (1993).
- [8] See also: G.C. Branco, P.A. Parada and M.N. Rebelo, Phys. Rev. **D52**, 4217 (1995); T. Han, R.D. Peccei and X. Zhang, Nucl. Phys. **B454**, 527 (1995).
- [9] W.-S. Hou and G.-L. Lin, Phys. Lett. **B379**, 261 (1996).
- [10] S. Bar-Shalom, G. Eilam, A. Soni and J. Wudka, Phys. Rev. Lett. **79**, 1217 (1997).
- [11] R. Cahn and S. Dawson, Phys. Lett. **B136**, 196 (1984); **136B**, 464(E) (1984); M. Chanowitz and M.K. Gaillard, Phys. Lett. **B142**, 85 (1984); G.L. Kane, W.W. Repko and W.B. Rolnick, Phys. Lett. **B148**, 367 (1984).
- [12] See e.g., O.J.P. Eboli, G. C. Marques, S. F. Novaes and A. A. Natale, Phys. Rev. **D34**, 771 (1986); S. Dawson and S. S. D. Willenbrock, Nucl. Phys. **B284**, 449 (1987); C.-P. Yuan, Nucl. Phys. **B310**, 1 (1988); R.P. Kauffman, Phys. Rev. **D41**, 3343 (1990).
- [13] See e.g., S. Dawson, Nucl. Phys. **B249**, 42 (1985); P.W. Johnson, F.I. Olness and W.-K. Tung, Phys. Rev. **D36**, 291 (1987); “Collider Physics”, V.D. Barger and R.J.N. Phillips, Addison-Wesley Publishing Company.
- [14] see e.g., D. Atwood, L. Reina and A. Soni, Phys. Rev. Lett. **75**, 3800 (1995); “The Higgs Hunter’s Guide”, J.F. Gunion, H.E. Haber, G. Kane and S. Dawson, Addison-Wesley Publishing Company.

- [15] D. Atwood and A. Soni, hep-ph/9607481.
- [16] See e.g. R. Frey, hep-ph/9606201, published in Iwate Linear Colliders 1995 p.144.
- [17] E. Jenkins, Phys. Rev. **D56**, 458 (1997).
- [18] D. Atwood and M. Sher, Report-no: WM-97-109, hep-ph/9707229 (and private communication).
- [19] S. Bar-Shalom and J. Wudka (in preparation); see also Ref. 18.
- [20] W.-S. Hou, G.-L. Lin and C.-Y. Ma, hep-ph/9708228.

Table 1: The scaled branching ratios $\text{Br}(t \rightarrow W^+W^-c)/\lambda^2$ and $\text{Br}(t \rightarrow ZZc)/\lambda^2$ in units of 10^{-6} for $m_H = 1$ TeV, $\tilde{\alpha} = \pi/4$ and for various values of m_t and m_h . The values of m_t and m_h are given in GeV.

	$\text{Br}(t \rightarrow W^+W^-c)/\lambda^2 \times 10^6$			$\text{Br}(t \rightarrow ZZc)/\lambda^2 \times 10^6$		
$\Downarrow m_t$	$m_h = 175$	$m_h = 185$	$m_h = 195$	$m_h = 175$	$m_h = 185$	$m_h = 195$
170	4.74×10^{-2}	1.15×10^{-2}	4.93×10^{-2}	/	/	/
175	0.411	5.71×10^{-2}	2.22×10^{-2}	/	/	/
180	34.9	0.202	6.68×10^{-2}	/	/	/
185	112	0.792	0.167	6.97×10^{-4}	9.88×10^{-3}	2.64×10^{-4}
190	216	26.0	0.398	3.03×10^{-2}	8.69	2.61×10^{-2}
195	336	82.4	1.15	0.121	28.8	0.313
200	466	158	20.7	0.282	55.9	12.8

Figure Captions

Fig. 1: (a) The Standard Model diagram for $e^+e^- \rightarrow t\bar{c}\nu_e\bar{\nu}_e$; (b) Diagrams for $e^+e^- \rightarrow t\bar{c}\nu_e\bar{\nu}_e(e^+e^-)$ in Model III.

Fig. 2: The cross-section $\sigma(e^+e^- \rightarrow t\bar{c}\nu_e\bar{\nu}_e + \bar{t}c\nu_e\bar{\nu}_e)$ in units of λ^2 as a function of m_h for $\sqrt{s} = 0.5, 1, 1.5$ and 2 TeV. $\tilde{\alpha} = \pi/4$ and we have set $\lambda = 1$ in the width $\Gamma_{\mathcal{H}}$.

Fig. 3: The cross-section $\sigma(e^+e^- \rightarrow t\bar{c}\nu_e\bar{\nu}_e + \bar{t}c\nu_e\bar{\nu}_e)$ in units of λ^2 as a function of $(\sin \tilde{\alpha})^2$ for $\sqrt{s} = 1$ TeV, $m_h = 250$ GeV and $m_H = 250, 1000$ GeV. λ as in Fig. 2.

Fig. 4: The ratio $R^{\nu\bar{\nu}tc} \left[\equiv \frac{\sigma(e^+e^- \rightarrow t\bar{c}\nu_e\bar{\nu}_e + \bar{t}c\nu_e\bar{\nu}_e)}{\sigma(e^+e^- \rightarrow \gamma \rightarrow \mu^+\mu^-)} \right]$ for $m_H = 1$ TeV, as a function of m_h for $\sqrt{s} = 0.5, 1, 1.5$ and 2 TeV. λ and $\tilde{\alpha}$ as in Fig. 2.

Fig. 5: The ratio $R^{\nu\bar{\nu}tc}$ for $m_H = 1$ TeV, as a function of \sqrt{s} for $m_h = 250, 350$ and 450 GeV. λ and $\tilde{\alpha}$ as in Fig. 2. See also caption to Fig. 4.

Fig. 6: The ratio $R^{tc/tt} \left[\equiv \frac{\sigma(e^+e^- \rightarrow \nu_e\bar{\nu}_e t\bar{c} + \nu_e\bar{\nu}_e \bar{t}c)}{\sigma(e^+e^- \rightarrow \nu_e\bar{\nu}_e tt)} \right]$ for $m_H = 1$ TeV, as a function of m_h for $\sqrt{s} = 0.5, 1, 1.5$ and 2 TeV. λ and $\tilde{\alpha}$ as in Fig. 2.

Fig. 7: The Feynman Diagram for $f\bar{f}' \rightarrow t\bar{c}V$ in Model III. For $e^+e^- \rightarrow t\bar{c}Z$, $V = Z$, $f = e^-$ and $\bar{f}' = e^+$.

Fig. 8: The cross-section $\sigma(e^+e^- \rightarrow t\bar{c}Z + \bar{t}cZ)$ in units of λ^2 as a function of m_h for $\sqrt{s} = 0.5, 1, 1.5$ and 2 TeV. λ and $\tilde{\alpha}$ as in Fig. 2.

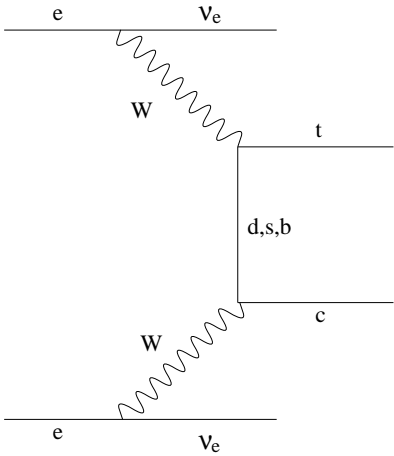
Fig. 9: The cross-section $\sigma(e^+e^- \rightarrow t\bar{c}Z + \bar{t}cZ)$ in units of λ^2 as a function of \sqrt{s} for $m_h = 200, 250, 300, 350$ and 400 GeV. λ and $\tilde{\alpha}$ as in Fig. 2.

Fig. 10: The cross-section $\sigma(e^+e^- \rightarrow t\bar{c}Z + \bar{t}cZ)$ in units of λ^2 as a function of $(\sin \tilde{\alpha})^2$ for $\sqrt{s} = 1$ TeV, $m_h = 250$ GeV and $m_H = 250, 1000$ GeV. λ as in Fig. 2.

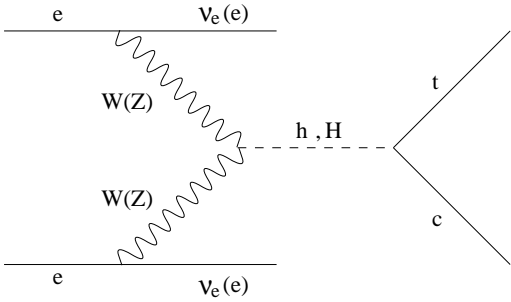
Fig. 11: The scaled branching ratio, $Br(t \rightarrow W^+W^-c)/\lambda^2$ as a function of m_h for various values of m_t . λ and $\tilde{\alpha}$ as in Fig. 2.

Fig. 12: The scaled branching ratios, $Br(t \rightarrow W^+W^-c)/\lambda^2$ and $Br(t \rightarrow ZZc)/\lambda^2$ as a function of m_t for $m_H = 1$ TeV and $m_h = 170$ and 185 GeV. λ and $\tilde{\alpha}$ as in Fig. 2.

Figure 1



(a)



(b)

Figure 2

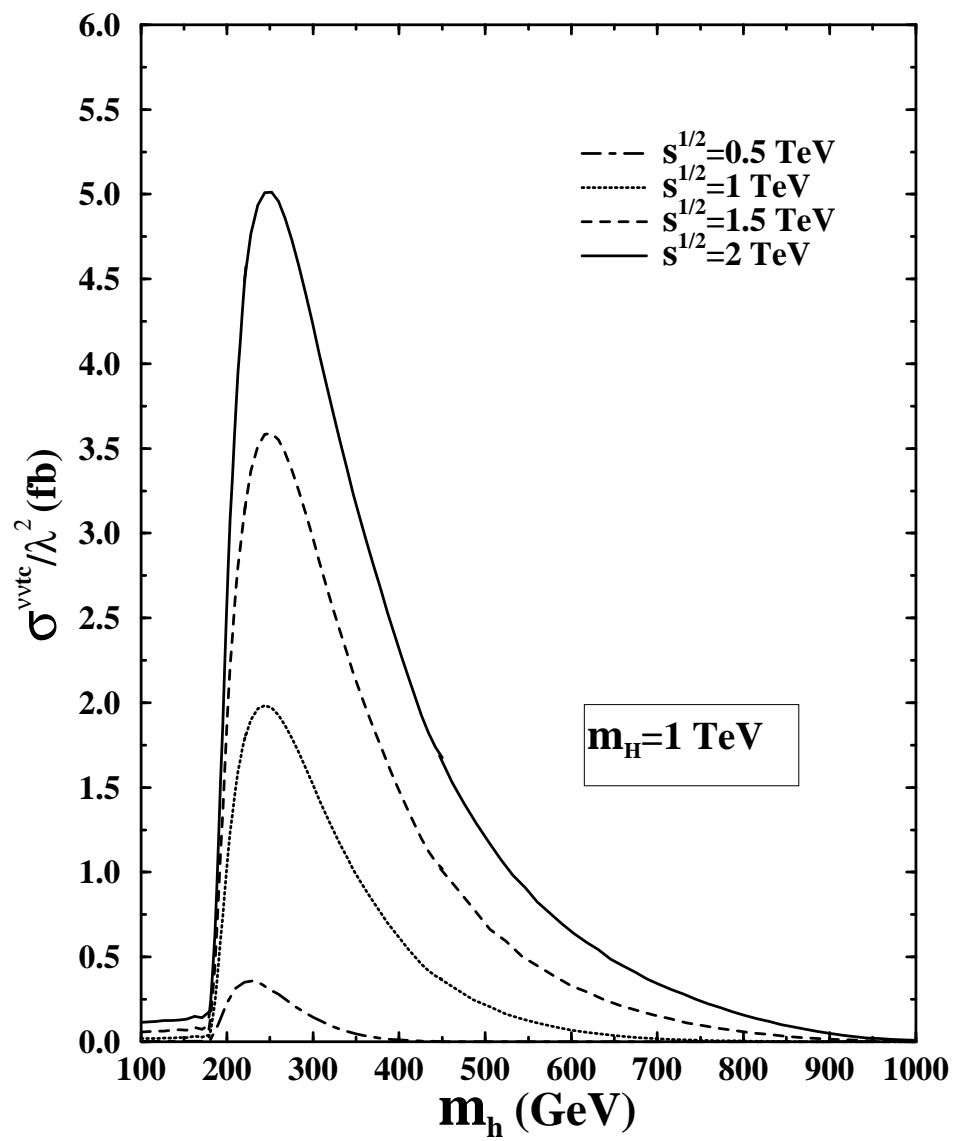


Figure 3

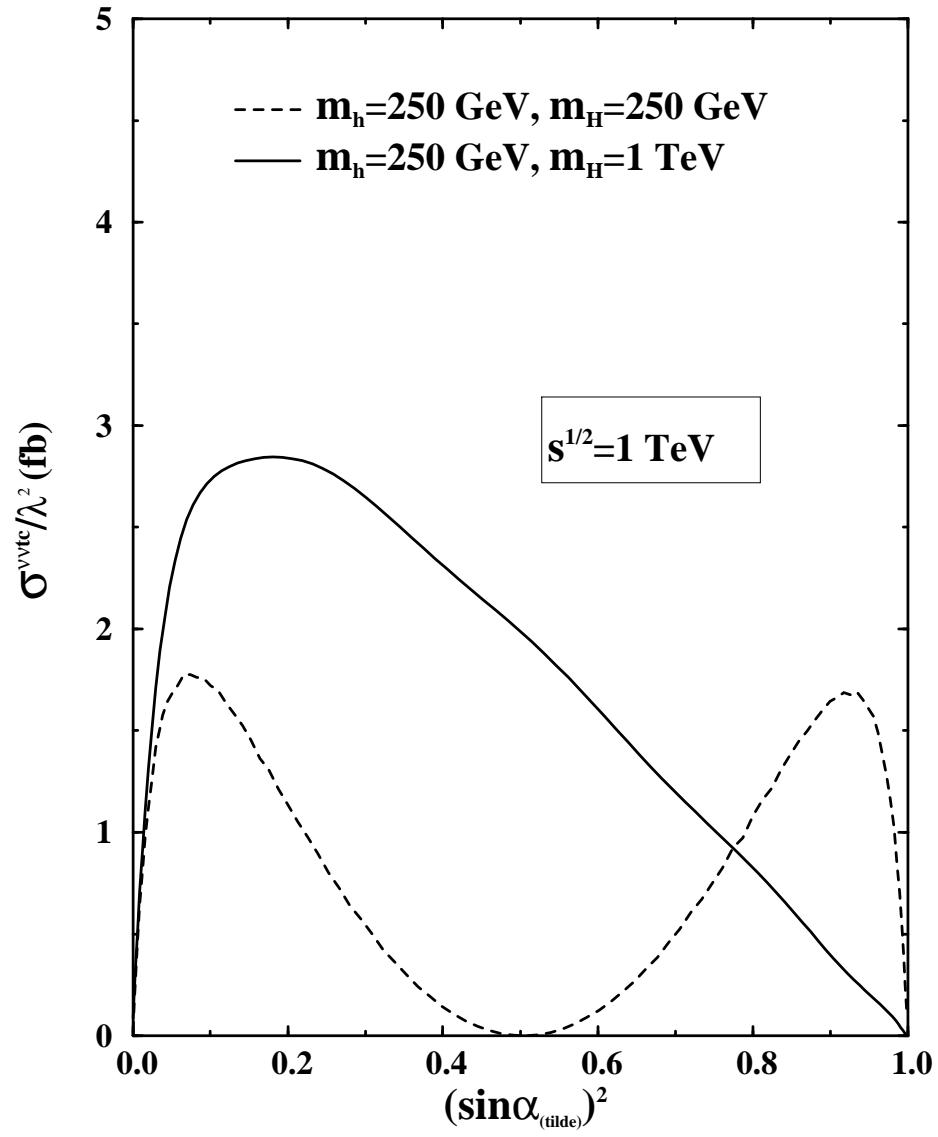


Figure 4

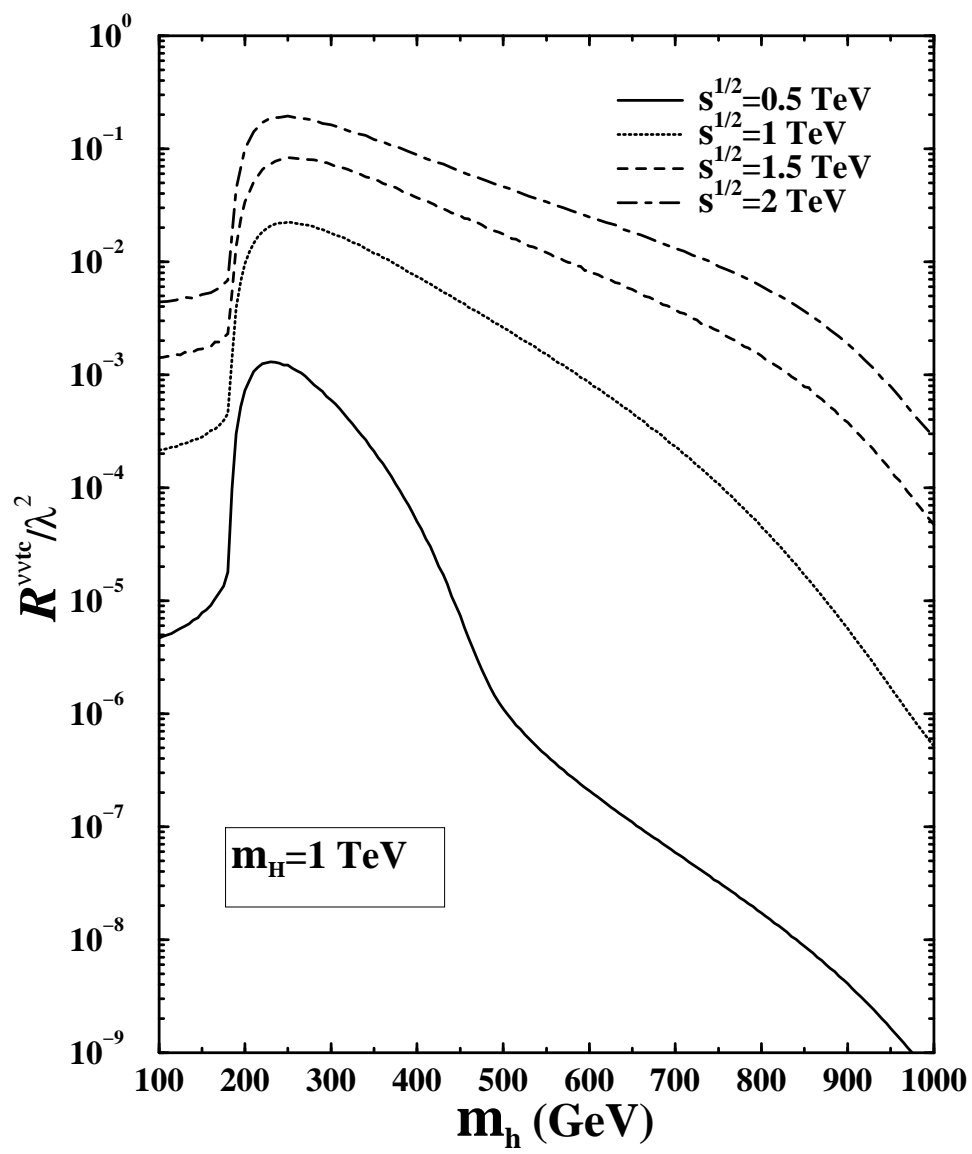


Figure 5

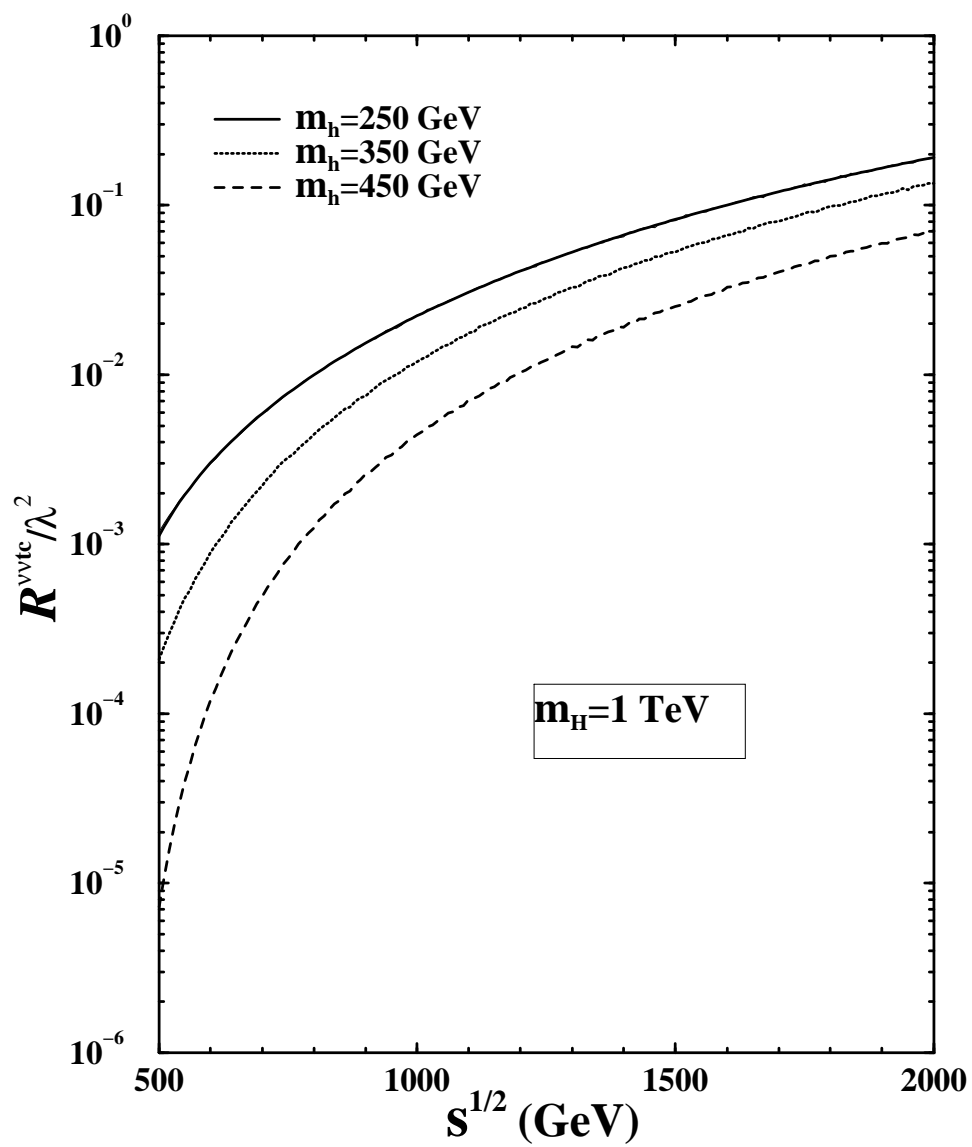


Figure 6

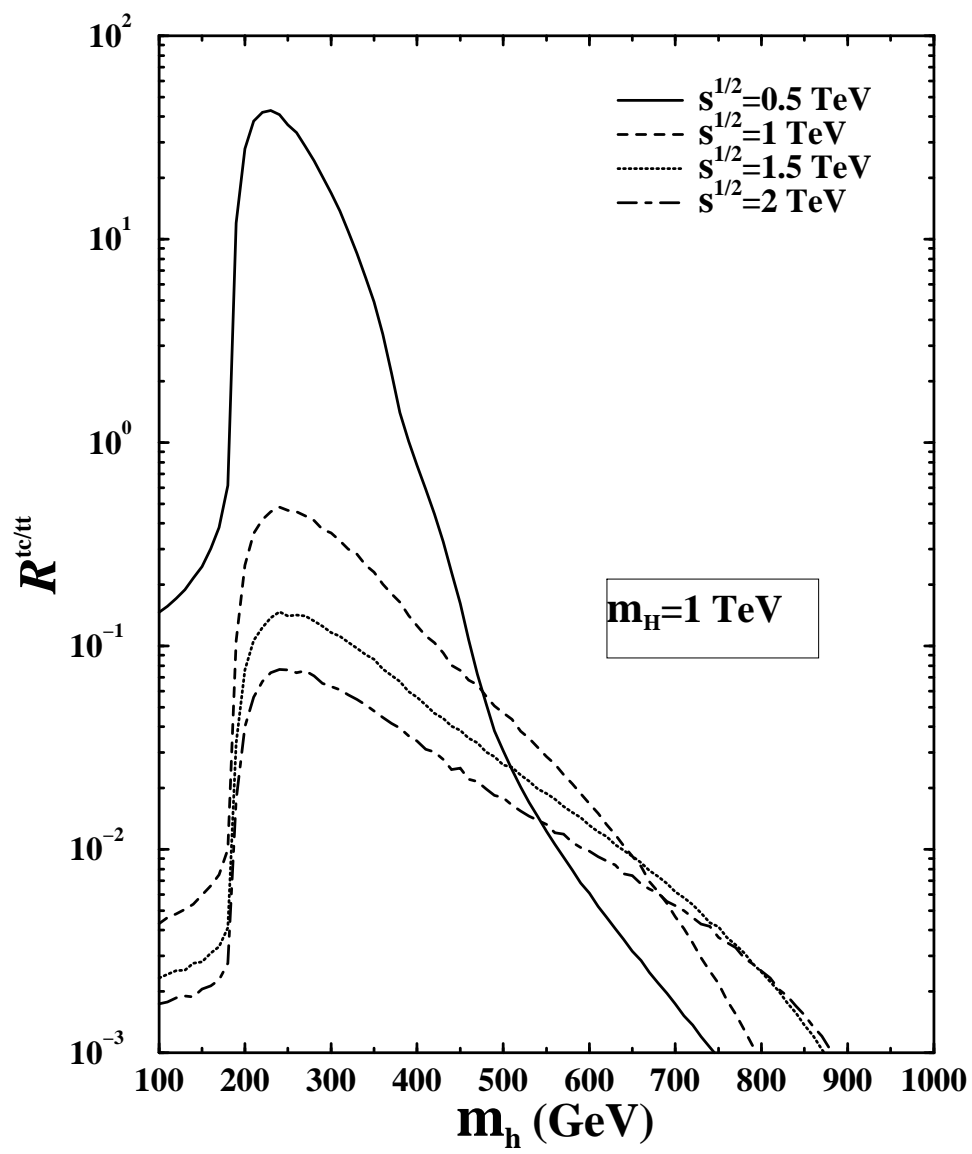


Figure 7

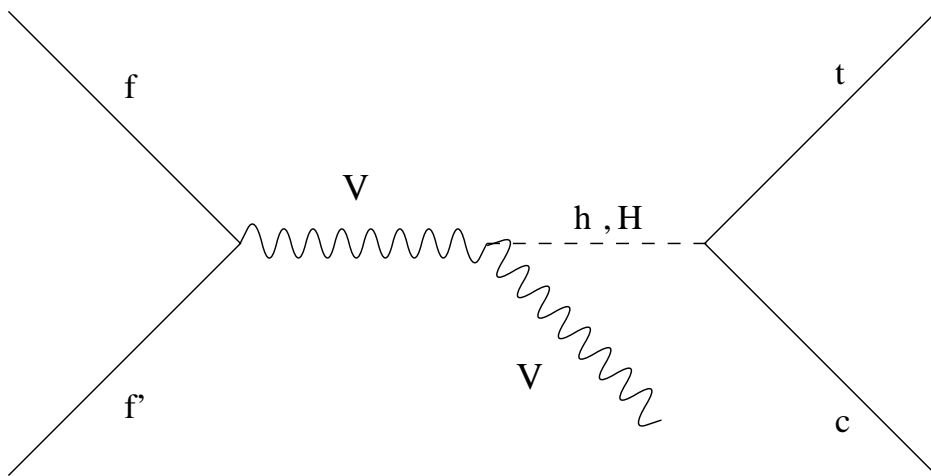


Figure 8

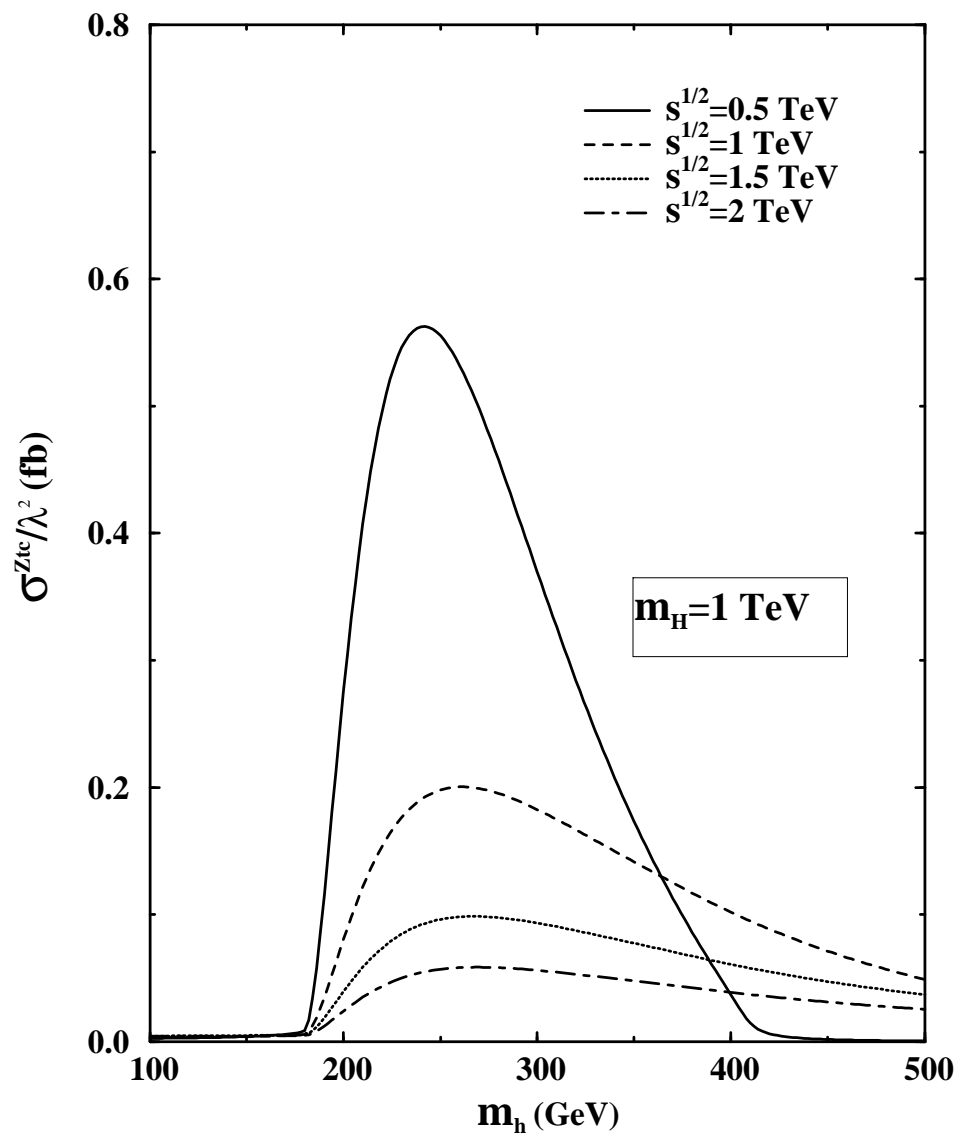


Figure 9

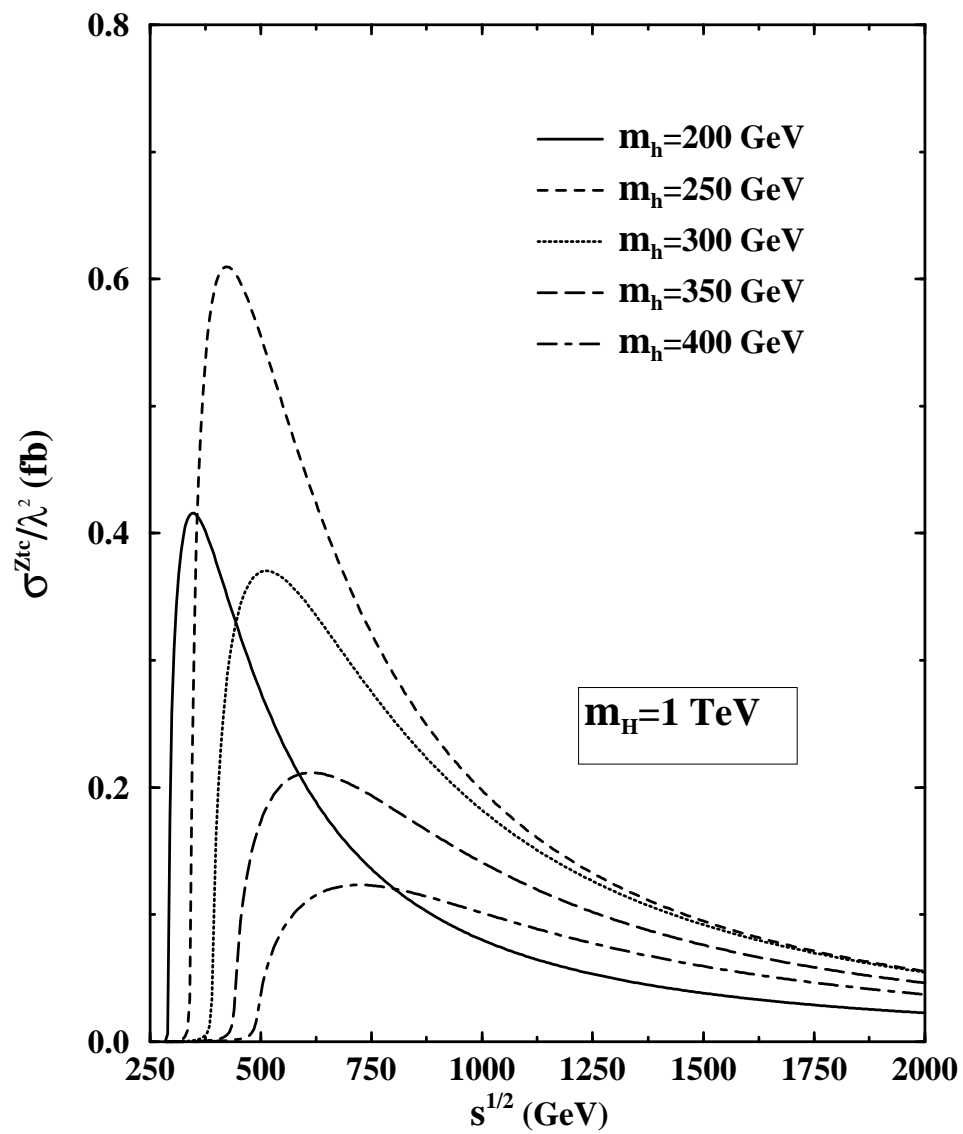


Figure 10

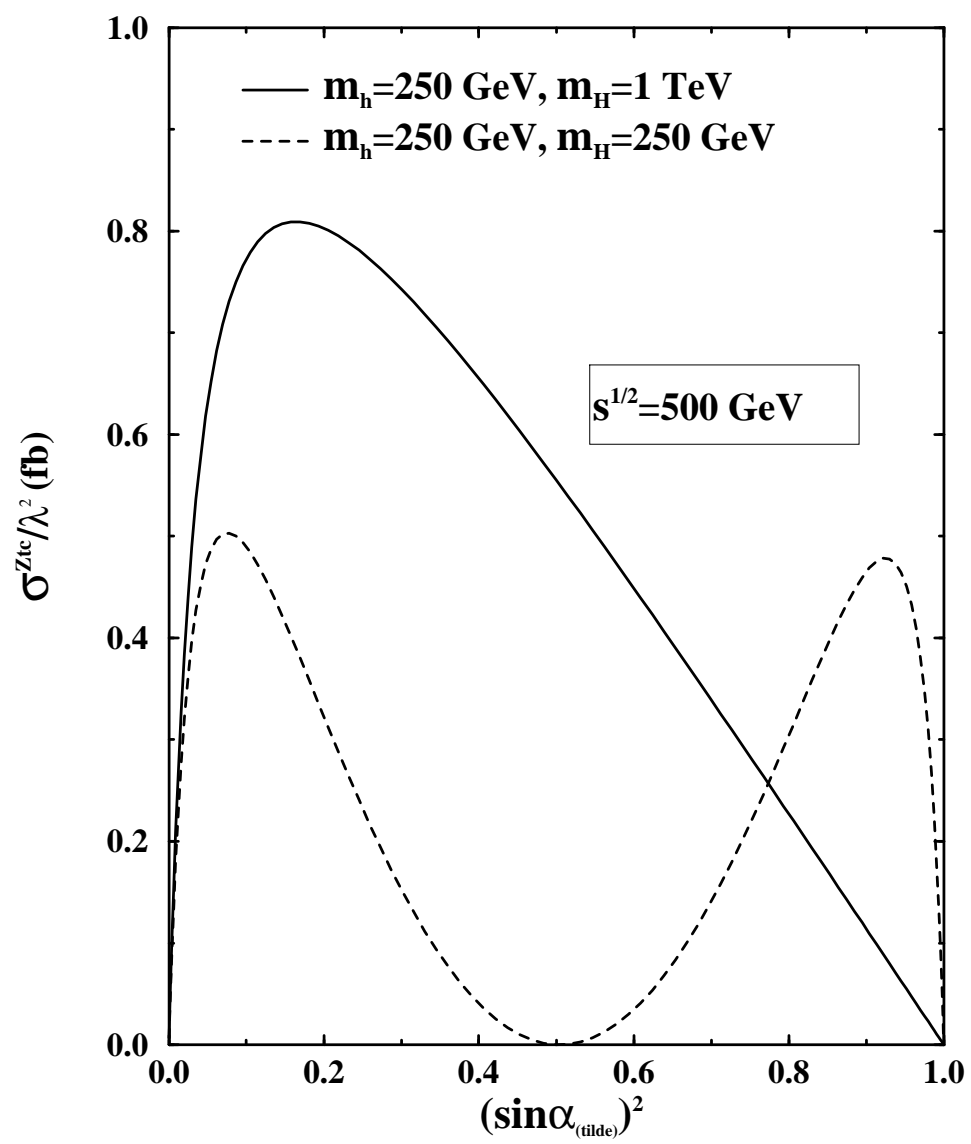


Figure 11

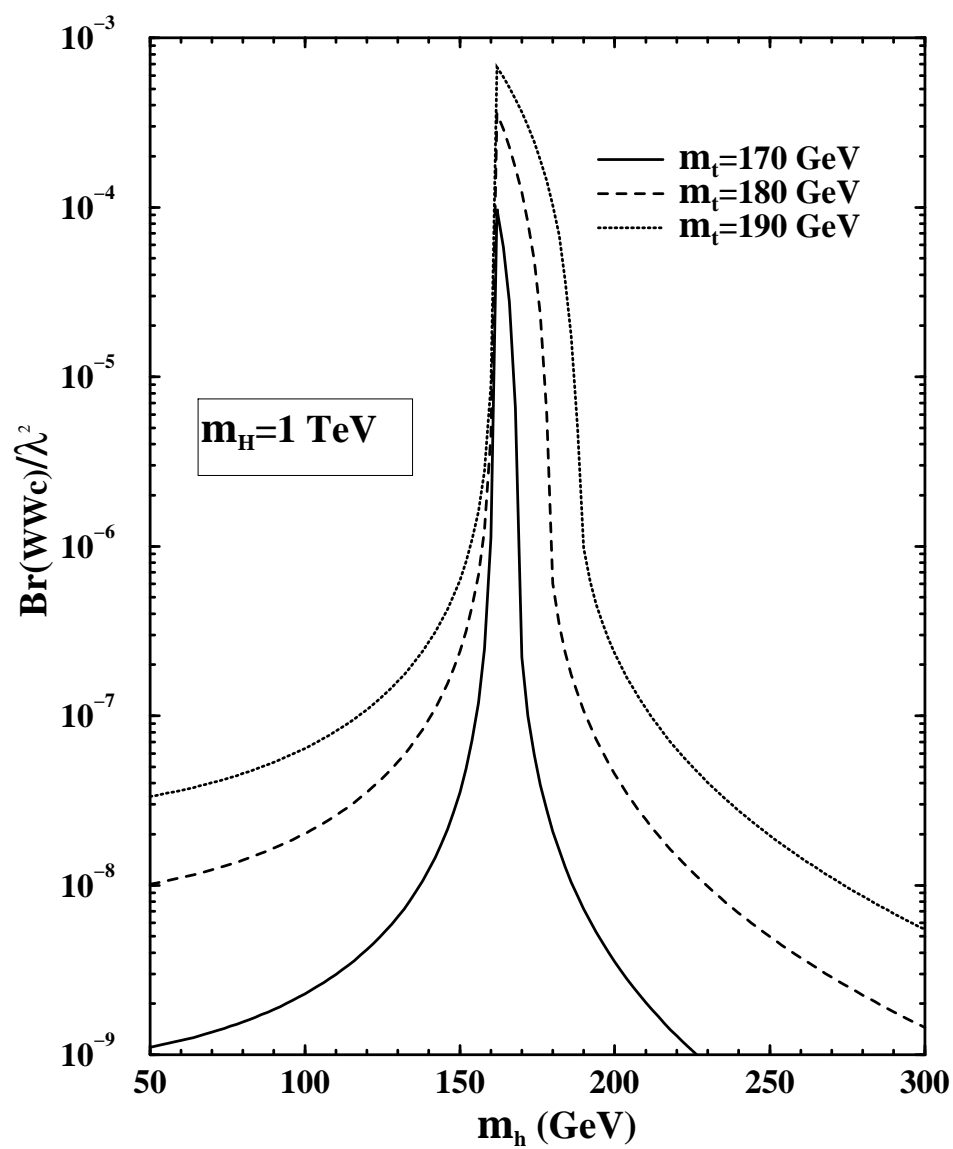


Figure 12

